Analytica Chimica Acta 716 (2012) 76–91

Contents lists available at SciVerse ScienceDirect

Analytica Chimica Acta

journal homepage: www.elsevier.com/locate/aca

Review

Synthesis and bioanalytical applications of specific-shaped metallic nanostructures: A review

Shiho Tokonami [a], Yojiro Yamamoto [b], Hiroshi Shiigi [b], Tsutomu Nagaoka [b,*]

[a] Nanoscience and Nanotechnology Research Center, Research Organization for the 21st Century, Osaka Prefecture University, 1-2 Gakuen-cho, Naka-ku, Sakai, Osaka 599-8570, Japan
[b] Department of Applied Chemistry, Graduate School of Engineering, Osaka Prefecture University, 1-2 Gakuen-cho, Naka-ku, Sakai, Osaka 599-8570, Japan

ARTICLE INFO

Article history:
Received 2 August 2011
Received in revised form 5 December 2011
Accepted 14 December 2011
Available online 21 December 2011

Keywords:
Metal nanoparticle
Nanostructure
Nanoparticle array
Detection
Biosensor

ABSTRACT

Many successful synthesis routes for producing different shapes of metallic nanostructures, including sphere, rod, cube, and hollow shapes, have been developed in the past few decades. Many applications using these nanostructures have been studied because the outstanding properties of the nanostructures are not exhibited by their bulk-state counterparts. This review paper reports some recent developments in clinical and biosensor applications. The first part focused on the synthesis methods of metallic nanostructures having various shapes along with their optical properties. The second and third part is an introduction of the gold nanoparticle assemblies and arrays, explaining the conjugation methods of metallic nanostructures with biological entities. The final part reviews on the recent bioanalytical applications using various shapes of metallic nanostructures.

Contents

* Corresponding author. Tel.: +81 72 254 9821; fax: +81 72 254 9821.
E-mail address: nagaoka@chem.osakafu-u.ac.jp (T. Nagaoka).

0003-2670/$ – see front matter © 2011 Elsevier B.V. All rights reserved.
doi:10.1016/j.aca.2011.12.025

Shiho Tokonami received her PhD degree at Osaka Prefecture University in 2007. She was a postdoctoral fellow at Hiroshima University, Tokyo University of Science Yamaguchi, and Osaka Prefecture University from 2007 to 2009. She is currently a special lecturer at Nanoscience and Nanotechnology Research Center, Research Organization for the 21st Century, Osaka Prefecture University. Her research area is nanotechnology and analytical chemistry, including a development of sensor for bio-associated materials.

Yojiro Yamamoto received his PhD degree at Osaka Prefecture University in 2007. His main research interest is a fabrication of electroless plating by using metallic nanoparticles. He has started his own company, Green Chem Inc., in 2010. He is currently a guest investigator at Graduate School of Engineering, Osaka Prefecture University.

Hiroshi Shiigi associate Professor of Applied Chemistry at Graduate School of Engineering, Osaka Prefecture University, was born in 1973. He received his PhD degree from Yamaguchi University in 2000. He worked at Yamaguchi University as a Research Associate (2000–2003). He joined Osaka Prefecture University as an Assistant Professor in 2003, and became an Associate Professor in 2008. His current research interest is the development of nanobioelectronics and biosensors based on the molecular recognition.

Tsutomu Nagaoka received his D.Sc. Degree from Graduate School of Science, Kyoto University in 1982 and became a Research Associate of Department of Applied Chemistry, Yamaguchi University. He became Associate Professor in 1990 and Professor in 2000. He moved to Osaka Prefecture University as Professor in 2003. At present, he is Professor at Graduate School of Engineering, Osaka Prefecture University. His research area includes analytical application of molecularly imprint polymers and metal nanoparticle material science.

1. Introduction

Metallic nanoparticles (NPs) have been examined for their use as tools for a new generation of technological devices, and many techniques for producing NPs are now available. These techniques essentially fall into three categories: physical methods, chemical syntheses, and mechanical processes, e.g., milling. In the last decade, many successful synthesis methods to produce metal nanostructures in a variety of shapes, such as sphere, spheroid, cube, octahedron, tetrahedron, bipyramid, plate, hollow, and rod, have been developed [1]. These nanostructures are usually synthesized by using a chemical method and have a variety of applications, such as electronic, magnetic, environmental, pharmaceutical, cosmetic, energy, optoelectronic, catalytic, and material applications, because of their outstanding properties that are not exhibited by their bulk-state counterparts [2–4]. In particular, NPs having a size of 1–100 nm exhibit unique properties that are not found in their bulk-sized counterparts and have been widely studied not only in the fields of electronics and photonics but also in the fields of disease marker detection, biomedical sensing, and environmental detection in the past few decades [5].

In the field of bioelectronics, biological events, such as deoxyribonucleic acid (DNA) hybridization and antigen/antibody reaction, change the interfacial properties of the electronic element, which enables the readout of the bioreaction by monitoring the performance change in the potential, impedance, surface resistance of electrodes, resonance frequencies of piezoelectric crystals, and field-effect transistors. In general, a combination of metallic nanostructures with biomaterials (target species) has enabled sensitivity enhancement, high throughput, and rapid detection in the recent years (Fig. 1).

This paper first discusses the basic characteristics of metal nanostructures having various shapes, including their synthesis methods, along with some recent developments in analytical and biological applications. After the introductory discussion, we discuss the assembling techniques on both substrates and biotemplates and describe the sensing system for biological entities as well as the enhancement of the sensitivity and selectivity of their system.

2. Synthesis of various shapes of nanostructure and their optical properties

2.1. Synthesis of gold nanoparticles

The high chemical stability and the straightforward synthesis and surface modification procedure of gold nanoparticles (AuNPs) have helped scientists and engineers expand the use of these NPs in a wide range of applications, such as cytologic staining, sensors, and electronics [6]. Many functionalized AuNPs have already become commercially available because of the growth of applications in the biological fields. The methods for synthesizing AuNPs currently include chemical, sonochemical, and photochemical routes. The chemical methods have several advantages over the other techniques because of their easy operation in the control of size and shape and in the functionalization of the particle surface by designing functional groups, which is absolutely imperative for certain specific sensor applications.

Citrate reduction is one of the best-known AuNP synthesis procedures among many other methods reported in the literature [7]. The most popular report is likely to be Turkevitch's 1951 paper, which describes the synthesis of ca. 20-nm AuNPs (Fig. 2A). The synthesis of AuNPs by using Turkevitch's method is simple and leads to an easy complex formation with DNA and antibodies. Briefly, sodium citrate used as a reducing agent is added to a boiling solution of chloroauric acid ($HAuCl_4$) stirred continuously for 20 min. The solution color then changes from pale yellow to purplish red, indicating that a particle with the above-mentioned size is produced in the solution. Although AuNPs synthesized by this method have often been used in biosensors and chemical sensors, the detailed mechanisms for the formation of AuNPs prepared by citrate reduction are unclear. Polte et al. have attempted to solve this problem by analyzing levitated sample droplets by small-angle X-ray scattering (SAXS) and X-ray absorption near-edge spectroscopy

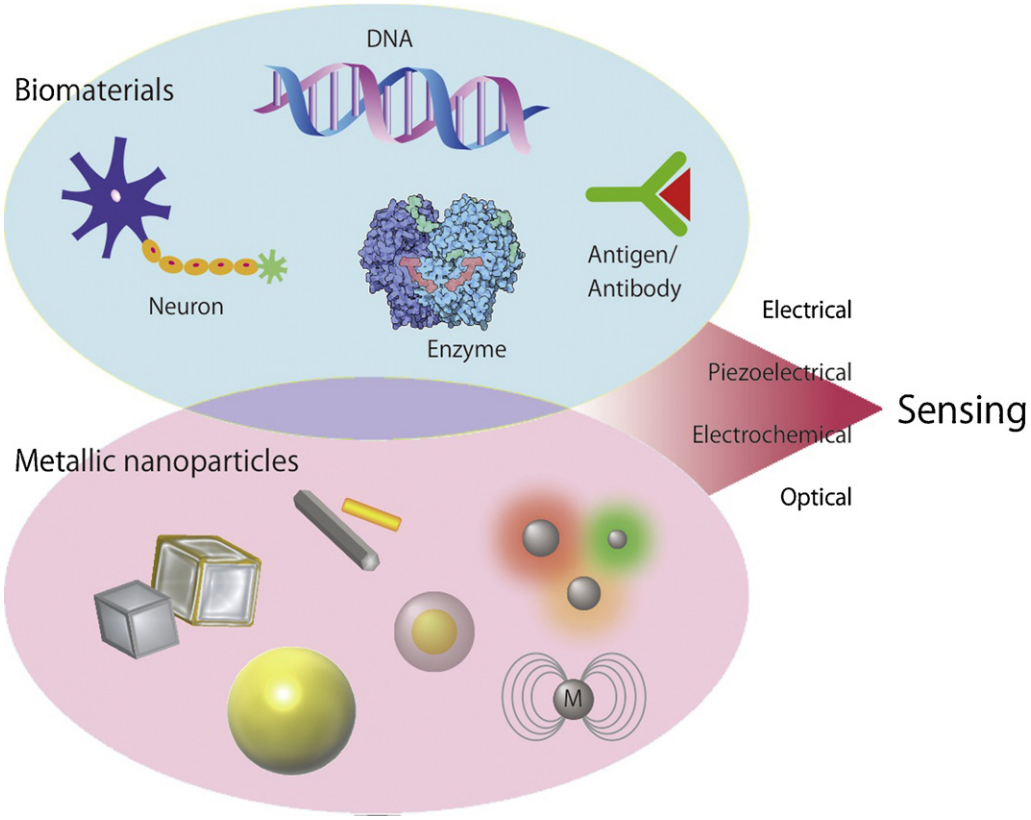

Fig. 1. Schematic representation of integrated biosensor fabricated by combining biomaterials with metallic nanoparticles.

(XANES) with synchrotron radiation, which allowed them to directly monitor precursor reduction and nanoparticle formation [8]. They have mentioned that the particles formed through a sequence of reaction steps consisting of a quick initial formation of small nuclei (step 1), coalescence of the nuclei into bigger particles (step 2), slow growth of particles sustained by the ongoing reduction of the gold precursor (step 3), and subsequent fast reduction ending with the complete consumption of the precursor species (step 4). The Brust method (two-phase synthesis and stabilization with thiol), published in 1994, also ranks high among synthesis techniques since it makes possible both control of particle diameter and grain-size distribution and also functionalization of the particle surface with thiol molecules. Furthermore, the Brust method has a considerable impact upon the thermal and air stability of synthesized particles with mean particle diameter of 1.5–5.2 nm [9,10].

In the past decade, substantial efforts have been put into the synthesis of rod-shaped AuNPs, or Au nanorods (AuNRs), in a high yield; these AuNRs exhibit good quality and uniformity (Fig. 2B). Various preparation routes have been reported, including the seed-mediated growth method [11], electrochemical method [12,13], and photochemical reduction method [14–17]. However, the seed-mediated growth method has been used more often than the other methods for obtaining a narrow distributed particle size because of its simple procedure and high-quality yield. The cetyltrimethyl ammonium bromide (CTAB), which is a cationic surfactant, is frequently used for obtaining nanorods in the presence or absence of silver nitrate [18–20]. A CTAB solution mixed with $HAuCl_4$ with an ice-cold sodium borohydride solution is used for producing a light-brown seed solution. The addition of the seed solution to a growth solution consisting of $HAuCl_4$, CTAB, and ascorbic acid can successfully produce the nanorods. The primary function of CTAB is to block crystal growth through its adsorption on a particular facet of the growth of seed particles. Recently, El-Sayed et al. have reviewed the detailed growth mechanisms for several different reported techniques [21]. When silver nitrate is used in the preparation, the amount of silver nitrate added dictates the final aspect ratio of the rods. The final aspect ratio can also be controlled by adjusting the rate of the spherical AuNP seed solution against the metal salt [20]. Biocompatibility is ensured by replacing CTAB with PEG [22,23] or other nontoxic ligands [24,25].

In addition, various shapes of Au nanocrystals such as octahedrons [26], tetrahedrons [27], icosahedrons [28], decahedrons [27], nanocubes [29,30], hexapods [31], and nanoflowers [32] have been synthesized by changing the reducing agent, capping agent, and solvent (Fig. 2C).

2.2. Synthesis of silver nanoparticles and nanocubes, and their use as a template to produce gold hollow nanostructures

Silver nanoparticles (AgNPs) have also been used as substrates for surface enhanced Raman scattering (SERS), optical labeling, and near-field optical probing [33–36]. AgNPs are generally prepared using $AgNO_3$ as a precursor and a reducing agent such as $NaBH_4$ or sodium citric acid. AgNPs have been used as a catalyst as well for various oxidation and oxidative coupling reactions, including formaldehyde production from methanol and air [37]. Ag nanocubes have been synthesized in ethylene glycol using polyvinylpyrrolidone (PVP) as a capping agent [38]. A rapid synthesis route to produce Ag nanocubes has also been reported in which oxidative etching was not necessary [39,40].

The preparation and characterization of hollow metallic nanostructures, often called nanocages and nanoframes, are one of the most fascinating subjects in current nanomaterial research. In fact, hollow gold nanostructures such as cages [33,41], rattles [42], and frames [43–45] have been synthesized via a galvanic replacement

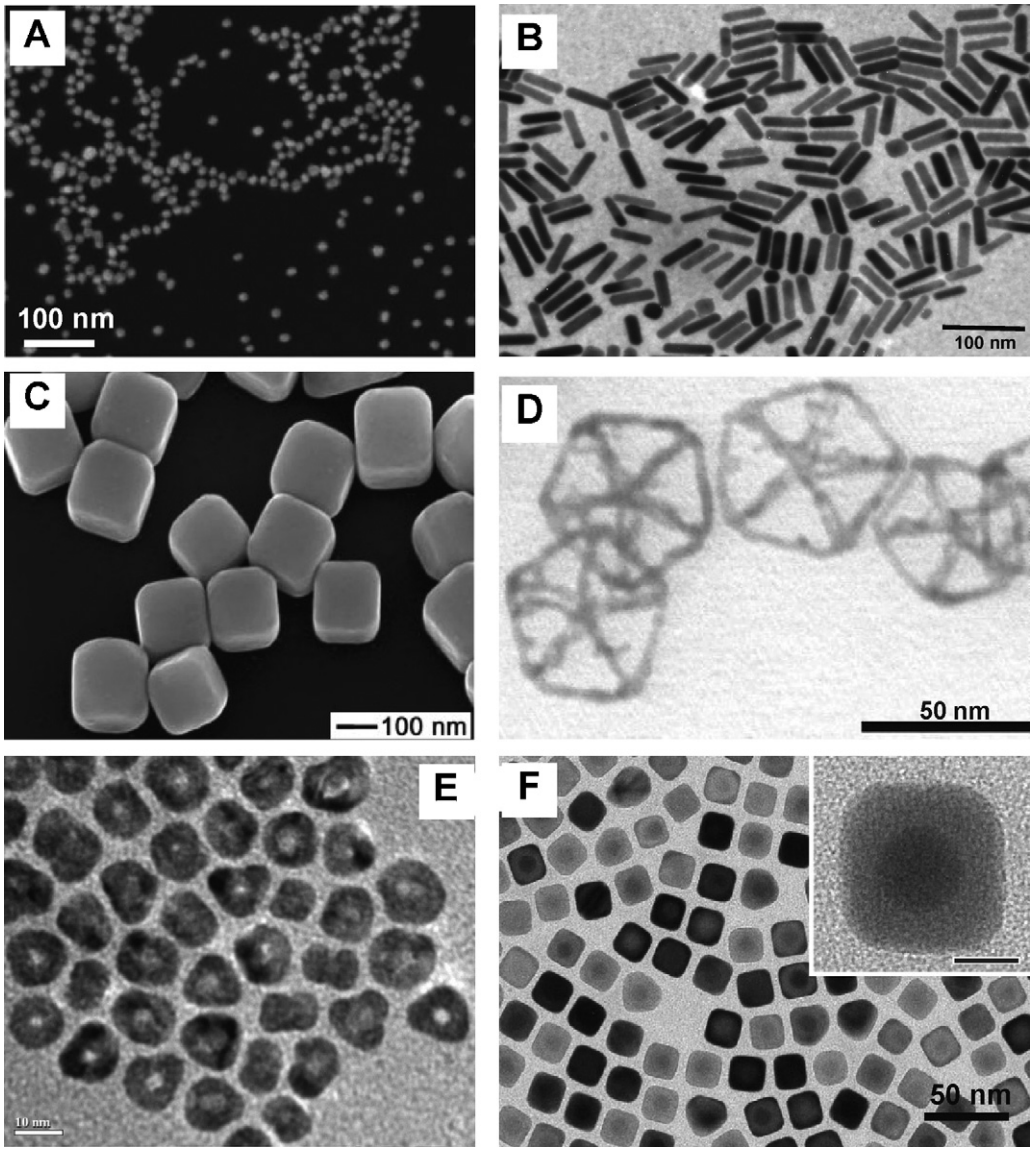

Fig. 2. TEM images of (A) gold nanoparticles, (B) gold nanorods, (C) silver nanocubes, (D) gold nanoframes, (E) AgAu core–shell nanoparticles, and (F) AuAg core–shell nanocubes.
Adapted from refs. [8,38,45,59] with permission from AAAS and ACS.

reaction in an aqueous solution (Fig. 2D). Among the hollow nanostructures, gold nanocages (AuNCs) are studied most widely because of the simplicity of their synthesis, tunability of the plasmon of gold shells and biocompatibility, etc. AuNCs have many potential applications such as catalysts, energy storage, optical and SERS sensors, drug delivery, and biomedical imaging. The unique features of AuNCs are not only their plasmonic characteristics but also their ability to act as functional nano-carriers/reactors.

AuNCs are synthesized by a galvanic replacement reaction, where Ag solid nanocubes are first used as sacrificial templates [46,41,47]. The addition of $AuCl_4^-$ to the Ag nanocube dispersion gives rise to the formation of a Au layer on the Ag surface, as shown by the two redox half-reactions below:

$$AuCl_4^- + 3e^- \rightleftarrows Au + 4Cl^- \qquad E^\circ = -0.99\ V$$
$$-)\ 3Ag^+ + 3e^- \rightleftarrows 3Ag \qquad E^\circ = +0.80\ V$$
$$AuCl_4^- + 3Ag \rightleftarrows Au + 3AgCl + Cl^- \qquad \Delta E^\circ = (+0.19 + 0.059 pK_{SP})\ V \text{ at } T = 298\ K$$

where K_{sp} is the solubility product of silver chloride. The free energy change of the total reaction is therefore negative, although the formation of the AgCl crystal, which hampers the replacement by the precipitation on the silver nanocubes, is usually carefully avoided. An increase in the amount of the Au complex leads to an increase in the hollow space in the Ag core since the deposition of a single Au atom on the Ag nanocube occurs at the cost of three Ag atoms (Fig. 3). As the amount of the added Au complex is increased, the evolution of the morphology of Au nanocages progressively occurs in the sequence of: (1) the pinhole formation on one of the six faces of each cube, (2) Au/Ag nanobox formation with a hollow interior, and (3) porous nanoframe formation [41]. Based on this method via galvanic replacement, not only Au but also Pt and Pd hollow

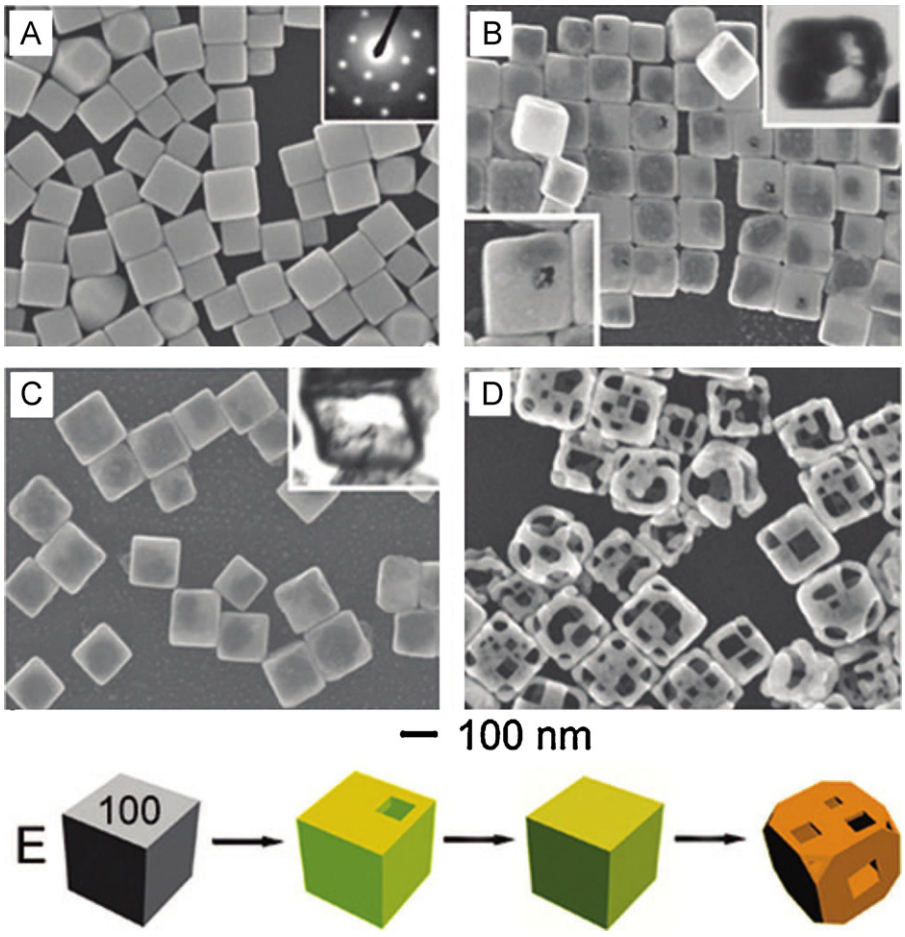

Fig. 3. SEM images of (A) Ag nanocubes with electron diffraction image (inset), (B) Ag nanocubes treated with 0.3 mL of 1-mM $HAuCl_4$, (C) Ag nanocubes treated with 0.5 mL of 1-mM $HAuCl_4$ (TEM image of the sample suggested the production of the hollow interior of the nanobox (inset)), (D) Ag nanocubes treated with 2.25 mL of 1-mM $HAuCl_4$ (porous nanocages were produced). (E) Illustration of the process of galvanic replacement to produce nanoboxes, nanocages, and nanoframes.
Reprinted with permission from ref. [41].

structures have been synthesized. Moreover, the one-step preparation method for Pd–Pt alloy nanocages with hollow interiors and porous walls has recently been reported by using Pd nanocubes, and their alloy nanocages showed an usefulness to a preferential oxidation of CO in excess hydrogen [48].

2.3. Synthesis of core–shell nanoparticles

Bimetallic NPs composed of two metal elements in a particle exhibit interesting electronic, optical, chemical, catalytic, and biological properties because of bifunctional or synergistic effects [49–54]. Among various structures of bimetallic NPs, the core–shell structure is scientifically interesting, particularly from the viewpoint of catalysis. In fact, core–shell bimetallic NPs have higher catalytic activity than monometallic NPs because the catalytic activity of shell atoms can be electronically affected by the core atoms [55,56]. For example, Ag/Au NPs having certain bimetallic compositions have been synthesized using two-phase (toluene–water) [57] and one-phase (water) [58] methods (Fig. 2E). In addition, the Au@Ag core–shell nanocubes in which the thickness of the Ag shell could be precisely tuned have been reported recently [59] (Fig. 2F).

Core–shell NPs have been reported to be a useful material for biosensing devices using fluorescence [60], electrochemical properties [61], magnetic properties [62–64], and LSPR [65,66]. Recently, Huang and co-workers reported a preparation technique of Au_2S/AuAgS/Ag_3AuS_2-coated AuNPs in which not only the size of the generated core–shell NPs but also the core size and shell thickness can be controlled [67]. The addition of a trace amount of Ag^+ to the AuNP- or AuNR-dispersed solution with $Na_2S_2O_3$ led to a significant red-shift in the plasmon wavelength owing to the formation of Au_2S/AuAgS/Ag_3AuS_2. They effectively used this form as a nanosensor for detecting Ag^+. Moreover, they found that the peak shift of AuNRs in the longitudinal plasmon wavelength was more sensitive than that of AuNPs.

2.4. Synthesis of hybrid nanostructures

Hybrid nanostructures of NPs with biological species or other materials have a great potential to increase performance in areas ranging from biomedical diagnosis and energy harvestings. In the recent photoluminescence imaging science, upconversion (UC) luminescence is expected to play a significant role since it offers high chemical stability, sharp emission bandwidths, and large anti-Stokes shifts, comparing to organic fluorophores and semiconductive NPs. Some lanthanide doped UC nanoparticles convert a near-infrared (NIR) radiation into a visible emission [68]. Wang et al. synthesized lanthanide doped nanocrystals ($NaYF_4$) in which dopant Gd^{3+} ion concentration in preparation changed their shapes from cubic to rod-like structure as well as their UC emission color [69]. The application of these nanocrystals as a biological label has been investigated by using $NaGdF_4$ as a host nanocrystal due to the higher relaxivities for MRI [70]. It successfully demonstrated the NIR-to-NIR UC luminescent and MRI dual-modal in vivo

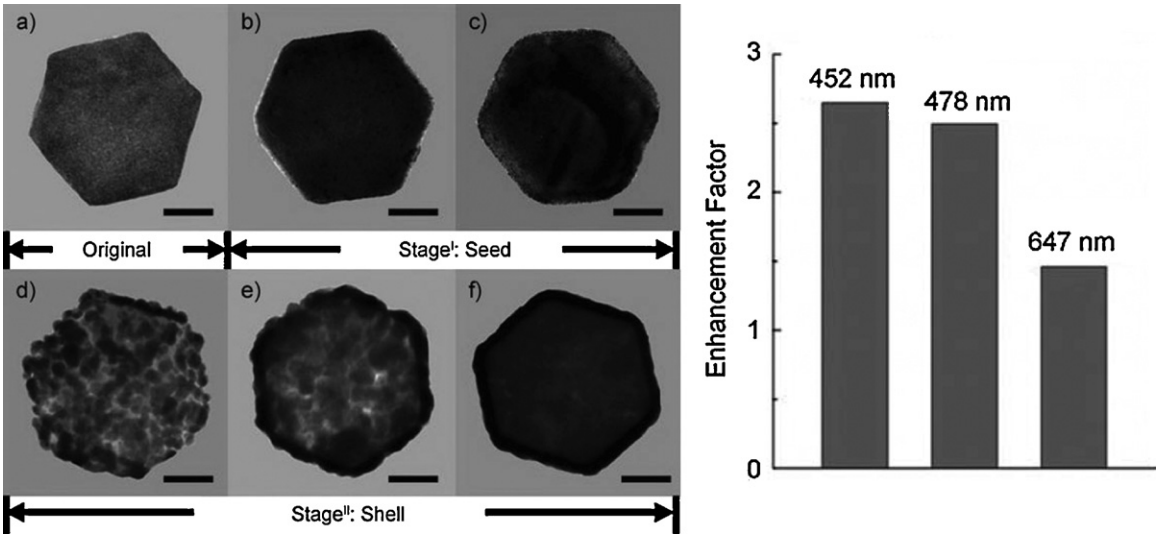

Fig. 4. TEM images of upconversion nanocrystals attached with Au nanoparticles and Au nanoshells. The bar graph indicates the emission enhancement factors induced by AuNP attachment.
Adapted from ref. [71] with permission from JWS.

imaging in mice. The formation of the hybrid nanostructure with such a rare-earth doped nanocrystals and AuNPs showed an enhancement in emissions. The AuNP immobilization method is different with each publication. AuNPs was prepared in advance and mixed with UC nanocrystals or Au precursor was mixed with citric acid in the presence of UC nanocrystals [71]. They suggested that the surface plasmon resonance of attached AuNP effectively coupled with excited fluorophores, leading to an increase in radiative decay rates, which brought a significant UC emission enhancement (~4 times) as shown in Fig. 4. Although the mechanism for such enhancement is still unclear, they would offer hope of progress in photonic, medical, therapeutic, and even in energy conversion.

On the other hand, nanoscale carbon materials, such as carbon nanotubes, fullerenes, and graphene have been attracted attention because of their unique structural and electrical properties. Carbon nanotubes assembled with metallic NPs have been utilized to enhance the sensitivity in electrochemical detection [72,73]. In fact, graphene has gained keen attention by many scientists since the Nobel Prize in Physics 2010 was awarded to their discovery. The graphene/inorganic hybrid materials have actively been investigated in Dai's group mainly for energy storage, electrocatalysis, and photocatalysis [74–76]. As for the biosensor, a unique chiral selective electrochemical sensing platform, graphen/mesoporous silica/AuNP hybrid structure, with taking advantage of aptamer and redox probe (ferrocene) have been reported [77]. The each component works to enhance the sensitivity. For example, the use of AuNP improves the immobilization amount of capture DNA, and mesoporous silica acts to avoid nonspecific adsorption of DNA. The sensor substrate is a little complicated, however, the system successfully discriminated D- and L-vasopressin with high detection limit of 5 ng mL^{-1}.

2.5. Microorganism-assisted synthesis of AuNPs

Both intracellular and extracellular microbial-assisted syntheses of metal nanoparticles (NPs) have been reported [78]. Nair and Pradeep reported that submicrometer-diameter Au, Ag, and Au/Ag alloy nanoparticles can be formed in bacteria by mixing $HAuCl_4$ and $AgNO_3$ with *Lactobacillus* strains [79]. A heterogeneous catalyst consisting of palladium NPs arrayed on a nanoscale biomagnetite support was also synthesized by using Fe(III)-reducing bacterium (*Geobacter sulfurreducens*). The resulting Pd-coated biomagnetite exhibited a high catalytic property for the Heck coupling of iodobenzene with styrene or ethyl acrylate [80]. The preparation method using living organisms could be a green chemistry approach that interconnects biotechnology and nanotechnology.

2.6. Optical properties of metallic nanoparticles

Noble-metal NPs, such as Au, Ag, and Cu NPs, have played an important role in the recent remarkable developments in nanoscience and nanotechnology. The dispersion liquid of each of these NPs exhibits various colors. AuNPs, in particular, exhibit a purplish red color in the dispersion state; in fact, the use of colloidal gold as a pigment to make ruby glass and stained glass dates back to the 4th century B.C. The Lycurgus Cup [81], now a possession of the British Museum, may be the most famous example. AuNPs have a broad absorption band in the visible region of the electromagnetic spectrum. Mie was the first researcher to formulate the nature of the optical band as a surface plasmon effect, in the so-called "Mie theory" [4,82]. The characteristics of the band arise from the collective oscillation of free-conduction electrons induced by an interacting electromagnetic field, and their resonances are noted as surface plasmon (Fig. 5a). In fact, the electric field of the incoming radiation causes the formation of a dipole in the NP. A compensation force for this dipole in NP results in a resonance wavelength, as shown in Fig. 5b. The specific resonance frequency depends on a number of parameters such as nanoparticle composition, morphology, concentration, solvent refractive index, surface charge, and temperature [34,83–86]. Meanwhile, such a resonance wavelength for rod-shaped NPs depends on the angle of the electric field. This results in two oscillations, transverse and longitudinal, that lead to two plasmon bands, as shown in Fig. 5c. The transverse SPR band occurs at a wavelength close to that of spherical AuNPs, while the longitudinal band is in the region 600–900 nm, depending on their aspect ratio (length/width).

3. AuNP assemblies and arrays

3.1. AuNP assembly and arrays on substrate

Assemblies of small building blocks such as atoms, molecules, and NPs into angstrom-scale and nanoscale structures, also called

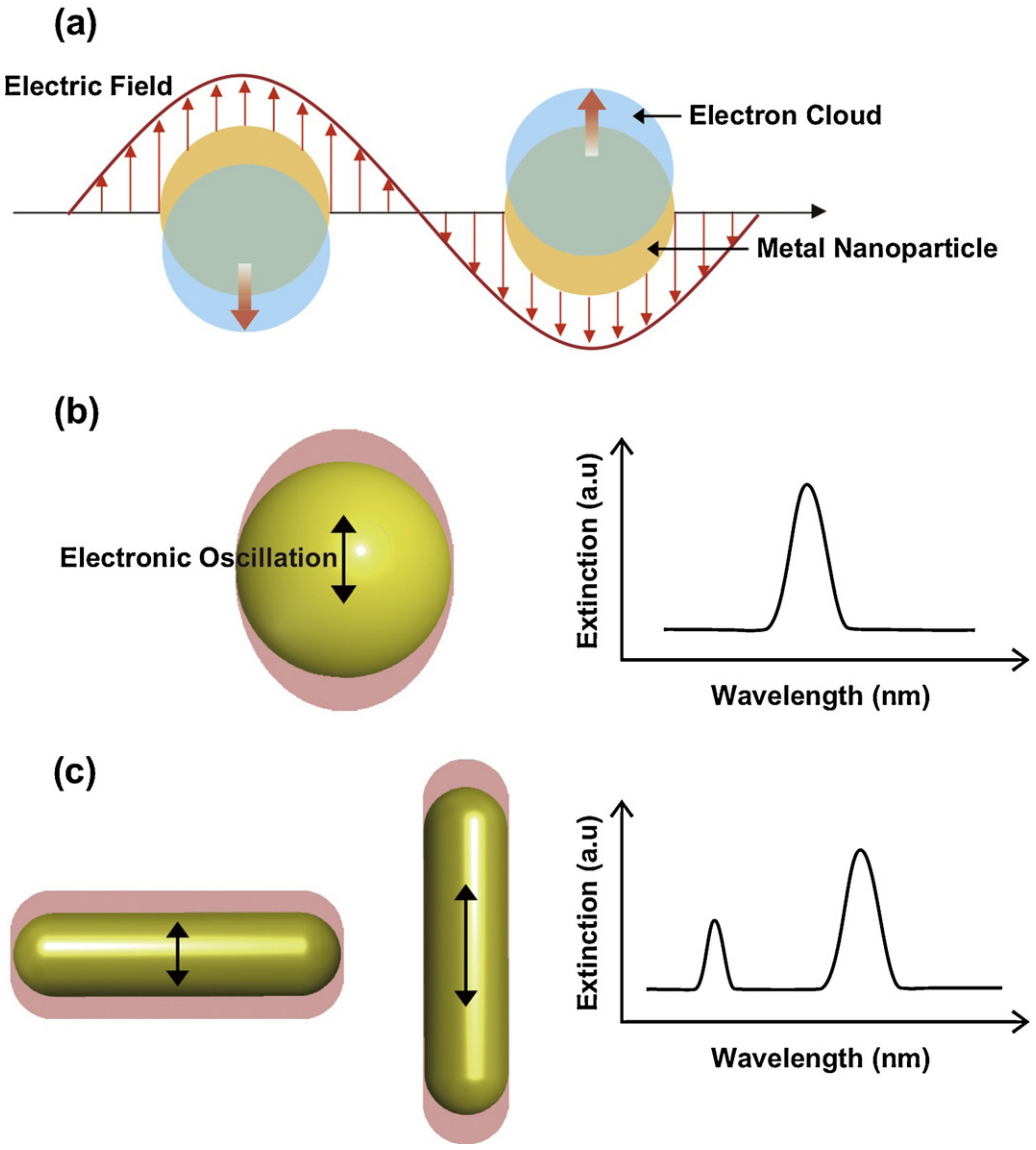

Fig. 5. Schematic representations of (a) localized surface plasmon resonance, (b) electric oscillation of nanosphere, and (c) nanorod with respective extinction spectrum.

bottom–up assemblies, are of critical importance in chemistry, biology, and materials science. This approach has brought in these disciplines a considerably smaller and more precise modeling format than the top down approach, which is typified by the lithography techniques [87]. Spherical NPs, for example, exhibit unique spectroscopic properties, such as surface plasmon resonance, and electro-catalytic properties, owing to their high surface areas, high edge concentrations, and different electronic states. The 2D or 3D structures of an AuNP assembly have been extensively studied because of their expected novel properties and been applied to chemical and biosensors. We have successfully fabricated AuNP assemblies via a self-organization mechanism in one-step using aniline as the reducing agent. The obtained shape was a raspberry-like aggregate [88] in water, while a mushroom-like aggregate [89] could be produced at the organic/water interface. Meanwhile, Song et al. fabricated sub-100-nm hollow AuNP superstructures using a peptide conjugate (C_6-AA-PEP_{Au}) [90]. Recently, assemblies of NPs in 1D polymer-like structures have been reported in which particles were bound into chains by the external field-induced attraction between colloids [91], chemical cross-linking, or physical attraction of ligands [92–94]. Nie et al. have reported the self-assembly of AuNRs coated with CTAB and thiol-terminated polystyrene molecules, as shown in Fig. 6 [95]. Moreover, they have effectively applied it to a step-growth polymerization of the arrow-head AuNRs and have shown that the kinetics and statistics of step-growth polymerization lead to a quantitative prediction of the linear, branched, and cyclic self-assembled structures [96].

The assemblies built on the conductive substrate work well in electrochemical experiments owing to the high conductivity between the substrate and the metal NPs. However, the low particle density obtained when the assembly is fabricated on an insulate substrate precludes electronic applications that require high particle-to-particle conductivity. To circumvent this problem, we have successfully assembled AuNPs on a plastic plate and on microbeads, made of polystyrene and polyethylene using alkylthiol as a binder [97–101]. The AuNPs assembled in this manner produce a single-layer film, and the conductivity of the AuNPs array ($4.8 \times 10^5\ \Omega^{-1}\ cm^{-1}$) is comparable to that of metallic bulk gold ($7.7 \times 10^5\ \Omega^{-1}\ cm^{-1}$), when the array is fabricated with a short alkylchain binder (butanethiol). In particular, note that the resistance of the film can be controlled from a very low value (typical of conductors) to high values (typical of insulators) solely by changing the length of the binder molecule. Such a particle deposited plastic surfaces exhibits electrocatalytic activities for H_2O_2, molecular

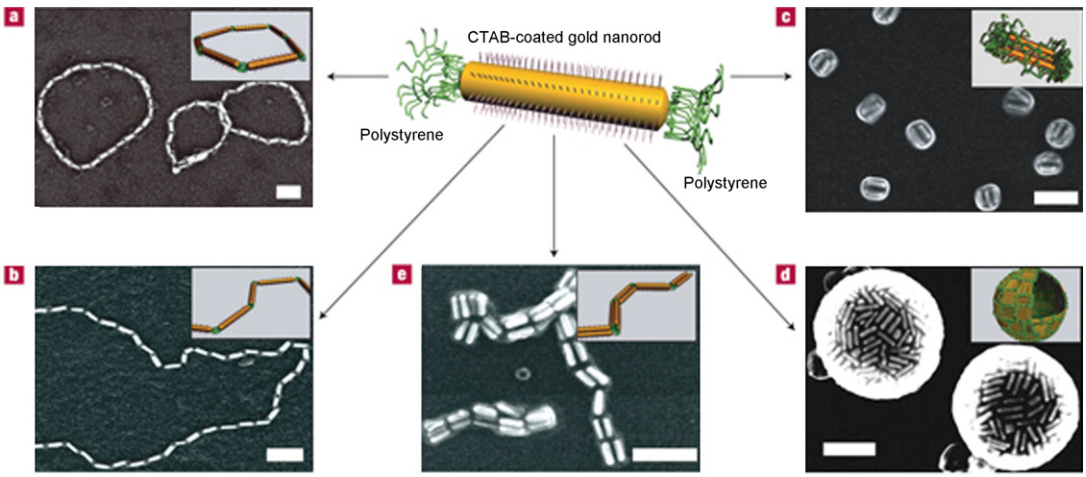

Fig. 6. Self-assembly of polymer-coated gold nanorods; the shapes of aggregates – (a) rings, (b) chains, (c) side-to-side aggregates, (d) nanosperes, and (e) bundled nanorod chains – can be controlled by selecting solvents.
Adapted from ref. [95] with permission from NPG.

oxygen, and organic amines [98]. Furthermore, the film prepared with butanethiol substantially attenuates the oxidation of ascorbic acid, indicating that this technique can be effectively applied to the electroanalysis of biochemical fluids.

3.2. Polarity of AuNPs and their assemblies on biotemplate

For the precise positioning of AuNP nanostructures, the interaction between the particles and substrate is one of the key factors, and the surface charge of AuNPs, therefore, plays a critical role. Most of the charges of metal NPs are fixed on the particle surface through the adsorption of a reducing agent in the preparation. Organic acid reductants, such as citric acid and ascorbic acid, yield negatively charged AuNPs; the anionic carboxylate added in the synthetic process adsorbs onto the surface of AuNPs as a protective layer, thereby imparting a negative charge. However, applications of metal NPs often need both negatively and positively charged AuNPs. For example, positively charged AuNPs are required for interaction with DNA, a polyanionic biomolecule. Typically, positively charged AuNPs are prepared by using the ligand exchange technique, in which the adsorbed anion is exchanged with cationic thiol through the following two-step controlled protocol. AuNPs are synthesized in an aqueous/organic solution interface and then adsorbed with the thiol molecule in organic media (step 1). The protectant layer is then exchanged or modified with a cationic thiol (step 2) [102,103]. The layer thus treated, however, provides only a low coverage of the cationic thiol on the surface of the nanoparticles. Hence, the nanoparticle must be modified with alkylthiols before the first step. In recent years, some studies have reported a simpler preparation technique for positively charged AuNPs that employs aniline as the reducing agent; the technique is a one-step process that does not require extra control, organic solvents, and ligand exchange [104,105]. It has been proposed that an aniline oligomer acts as a protectant of AuNPs from the observation of UV–vis spectra and conductivity measurements of an AuNPs film cast on the microelectrode.

It has also been suggested that positively charged nanoparticles are easily carried into a living cell, which provides a means for gene delivery. Nakao et al. have succeeded in fixing DNA strands straight onto a glass surface without any sophisticated equipment [106]. Using DNA as a template, they have created a DNA nanowire out of aniline-protected and positively charged AuNPs as described above (Fig. 7) [107]. Furthermore, they have minutely investigated the spectroscopic properties of aligned NPs [108]. Warner and

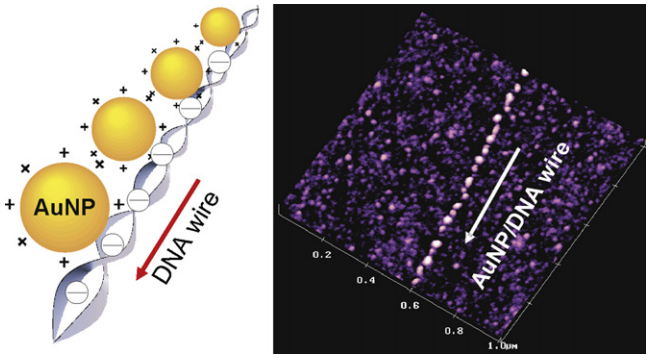

Fig. 7. Illustration of a gold nanoparticle highly ordered on a substrate by using electrostatic interaction of straightened DNA and aniline-coated positively charged gold nanoparticles. AFM image shows that gold nanoparticles are highly arranged in one dimension on the substrate.
By courtesy of Dr. Nakao, ref. [108].

Hutchison have assembled AuNPs into lines, ribbons, and junctions (such as Y-shaped 2D structures) templated with DNA, using positively charged AuNPs synthesized from a triphenylphosphine-passivated precursor-nanoparticle by a biphasic ligand exchange reaction with thiocholine (N,N,N-trimethylaminoethanethiol iodide) [109]. An interesting report on 2D AuNPs arrays fabricated by taking advantage of DNA hybridization is introduced as another example. The programmable DNA sequences provide multiple 2D nanocomponents consisting of AuNPs having different particle sizes. The technique differs from the two reports mentioned above in that it uses the hybridization reaction instead of the charge interaction between AuNPs and DNA [110]. First, the researchers assembled a scaffold consisting of a set of 22 DNA strands. The hybridization of DNA that was immobilized on 5- and 10-nm AuNPs, with the hybridization sites arranged on the DNA scaffold, provided an ordered array of AuNPs having lines of large and small nanoparticles.

4. Conjugation of specific-shaped metallic nanostructures to biological entities

4.1. Covalent attachment

It is necessary to functionalize surface of metallic nanostructure with biomolecules for further biological applications. The

covalent attachment is one of the most direct methods to bind a biomolecule to the surfaces. Among them, thiol groups (—SH) have been frequently used because they provide an efficient means of chemisorption of molecules onto the coinage surfaces. The biomolecules such as DNA [111] and peptide [112] have been conjugated due to the thiolate–gold linkage for their analysis. The thiol molecule introduction to the target fixing material enables us to immobilize not only biomolecules but also polymers to the metallic nanostructure surface. For example, Xia and coworkers have successfully fixed thermally responsive polymers making use of Au–thiolate bonding to control the release of drug with NIR laser irradiation or high-intensity focused ultrasound by using Au nanocages [113,114].

Meanwhile, heterobifunctional crosslinkers such as EDC (1-ethyl-3-[3-dimethylaminopropyl]carbodiimide hydrochloride) have also been utilized to induce bonding between primary amines and carboxyl groups. This cross-linking method enabled us to immobilize biomolecules onto the Au nanostructure surfaces on the basis of the EDC/NHS (N-hydroxysuccinimide) chemistry [115,116].

4.2. Noncovalent attachment

An electrostatic adsorption is one of the examples of noncovalent attachment between Au nanostructures and biomolecules. NPs have usually been covered by anionic ligands such as carboxylic acid derivatives. Such a negatively charged NPs easily interact with positively charged biomolecules. Of course, the opposite case in which positively charged NPs attract anionic biomolecules is conceivable. With regard to proteins including antibodies, they consist of few dozens of amino acids. The positively charged amino groups have an important role for conjugation with metallic NP. Many AuNP synthesized by citric acid as a reducing agent are negatively charged due to the citrate ion stabilizer. Therefore, antibodies such as IgE and IgG can be easily attached to the AuNP or AgNP surface with electrostatic interaction [117]. On another front, thiol groups, e.g. cysteine residues, contained in some proteins provoke a Au–thiolate chemical adsorption. The strategies to conjugate metal nanostructures with biomolecules are summarized in Fig. 8.

5. Bioanalytical applications using specific-shaped metallic nanostructures

5.1. Biosensors using AuNP

One of the outstanding properties of AuNPs is their high visibility; in contrast to the extinction coefficients of fluorescent molecules (e.g., fluorescein, $9.2 \times 10^4\ M^{-1}\ cm^{-1}$ in ethanol at 483 nm), 40-nm AuNPs exhibit an extinction coefficient of $2 \times 10^9\ M^{-1}\ cm^{-1}$. This high extinction coefficient results in an enhanced detection sensitivity of approximately 2.2×10^4 fold [118]. In addition, AuNPs exhibit the property of surface modification through self-assembly with thiols and/or amino groups, thereby adding surface functionality to the particles; such particles have been used as functional probes. Another feature of AuNPs is the color change due to aggregation. AuNPs often carry a negative charge, which stabilizes their particle dispersion in the solution. The color change caused by aggregation can be efficiently used for recognizing the interaction between a receptor-modified nanoparticle and an analyte by the removal of particle charge or the formation of an interconnected structure, AuNP–analyte–AuNP; these interactions produce a measurable color change due to long-range plasmon coupling [119]. The optical biosensor based on AuNP aggregation induced by bioreaction such as DNA hybridization, enzyme reaction, and peptide bonding, developed first by Mirkin and co-workers, has remained famous [120–122]. The applications based on their findings have spread over a wide range, such as the detection of toxins, heavy metals, and environmental pollutants in recent years [123–128]. These colorimetric sensors have helped take an important step towards real-time sensing because the signal is detectable by the naked eye without sophisticated instruments. A lateral-flow-based immunochromatograpy

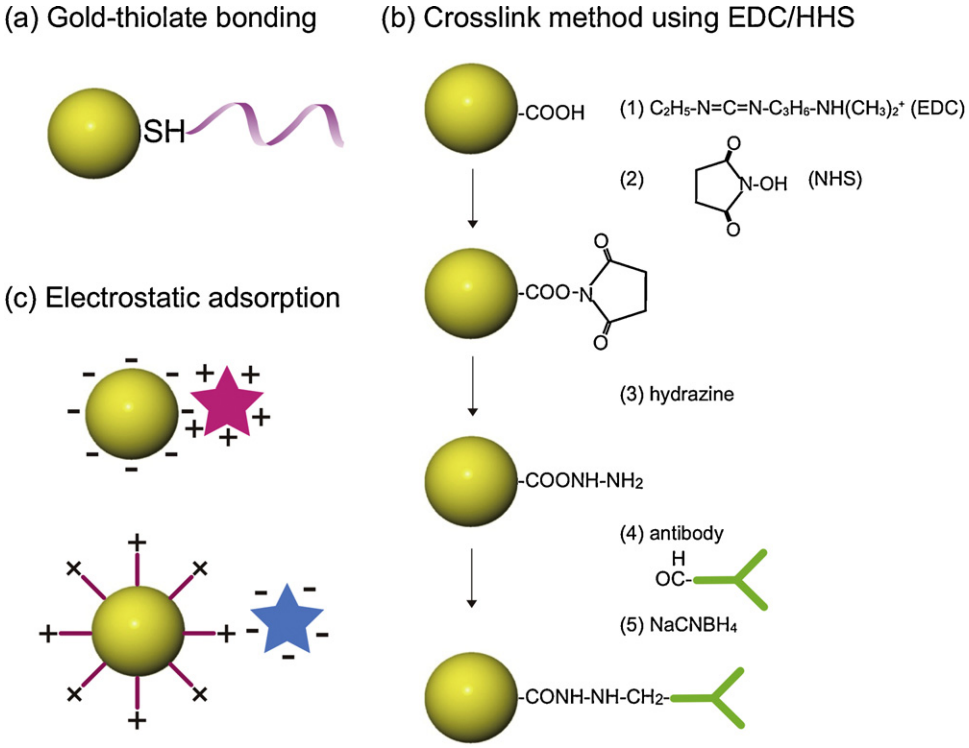

Fig. 8. Summary of the strategies for the conjugation of metallic nanostructures with biological entities.

combined with AuNPs provide rapid, simple, and low-cost detection. Such a detection system usually consists of a sample pad, conjugation pad, test line, control line, and absorption pad, which enable us to determine proteins [129], DNA [130], heavy metal ions [131], and toxins [132]. In fact, some AuNPs are already used for testing for prostate-specific antigens (PSAs) and influenza and have been commercialized by several companies.

Another striking property of AuNPs is that AuNPs whose particle size exceeds ca. 10 nm work as effective fluorescence quenchers [133]. The quenching is generally induced when the AuNPs are located close (less than 2 nm) to the fluorophore because of the fluorescence resonance energy transfer (FRET). The efficiency of these fluorescence quenchers is considerably larger than that of conventional organic quenching substrates. Hence, various types of analyses based on the recovery of fluorescence have been carried out for DNA and metal ions [119].

Meanwhile, the plasmon coupling induced by single pairs of metal nanoparticles has often been investigated by using dark-field optical microscopy. It's commonly used in a biological field since the high contrast images can be obtained even in a simple setup. A condenser, having a larger numerical aperture than that in the objective lends, is used in the dark-field microscopy. Therefore, no direct light from the condenser enters the objective lens, and only the light that is scattered by the sample enters the objective. A single spherical AuNPs are observed as green color in general, yet the color changes to be red after dimmer or trimmer formation due to the near-field coupling [108]. This color change is tuned by the particle distance, as is the case with the bulky aggregation mentioned above. This phenomenon has effectively used to measure distance in a nanometer scale [134–136]. The limited detection distance within 10 nm in FRET measurement is a crucial disadvantage, however, using a particle–particle plasmon coupling enables us not to consider it anymore, which is a great advantage because it can be used for all types of biological target species. With this significant advantage, a continuous observation of caspase-3 activity was accomplished in living cells (Fig. 9). This method is expected to open the way for the investigation of single-molecule activities in living cells in the future.

5.2. Biosensors and bio-applications using AuNRs

AuNRs produce a strong evolution of surface plasmon absorption band in the range of the visible and near-infrared (NIR) regions. Because of the longitudinal SP bands in the NIR regions, the AuNRs are expected to be novel functional materials for analytical [137,138], photofunctional [139,140], photothermal therapy [141–143], and biochemical [144–147] applications. Meanwhile, the plasmon coupling among metallic NPs has been employed for enhancing optical signals, including Raman [148,149], second-harmonic [150], fluorescence [151], and two-photon photoluminescence [152], and applied in photolithography [153], two-photon polymerization [154], and nanometric optical tweezers [155]. Wang et al. [156] and Thomas and Pramod [157] investigated the plasmon coupling of AuNRs in dimmers at their ends with various angles. As an application for sensing, AuNRs were designed to form side-by-side and end-to-end assemblies for the detection of the environmental toxin microcystin-LR (MC-LR) [158]. The aggregation patterns were proficiently changed by controlling the modification portion of MC-LR OVA and antibody to MC-LR, as shown in Fig. 10. The original optical properties of the AuNRs were changed according to the assembling patterns (see the respective UV–vis spectra in Fig. 10C and D). Interestingly, an end-to-end aggregate resulted in better sensitivity and detection ranges.

In addition, AuNRs may have been used as ultraefficient energy quenchers because their immense absorption coefficients were 10^4 fold to 10^6 fold higher than those of conventional organic dyes [159,160]. Therefore, AuNRs have been receiving considerable attention in applications not only in imaging but also in photothermal therapy because of the absorbance in the NIR region [161–164]. The NIR light, in particular, provides deep-tissue penetration with high spatial precision without damaging normal biological

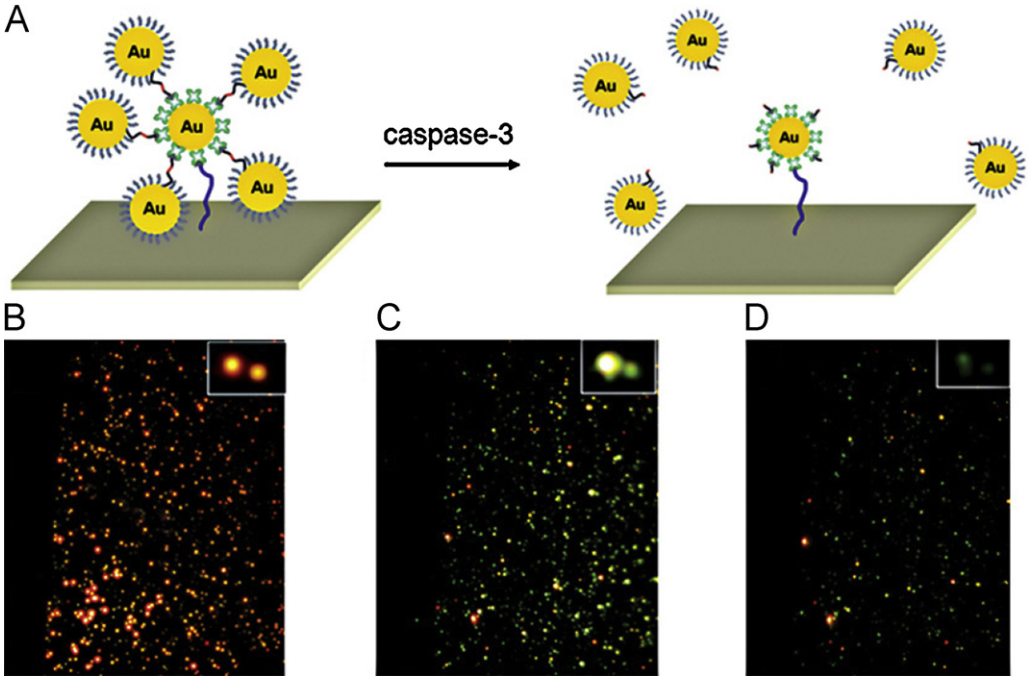

Fig. 9. (A) Schematic illustration of crown nanoparticle plasmon rulers for the observation of Caspase-3 activities. (B–D) Scattering color of the nanoparticles observed by using dark-field microscopy. Initial red colored spots changes to be yellow and then green by the addition of caspase-3. (For interpretation of the references to color in this figure legend, the reader is referred to the web version of the article.)

Adapted from ref. [135] with permission from National Academy of Science, USA.

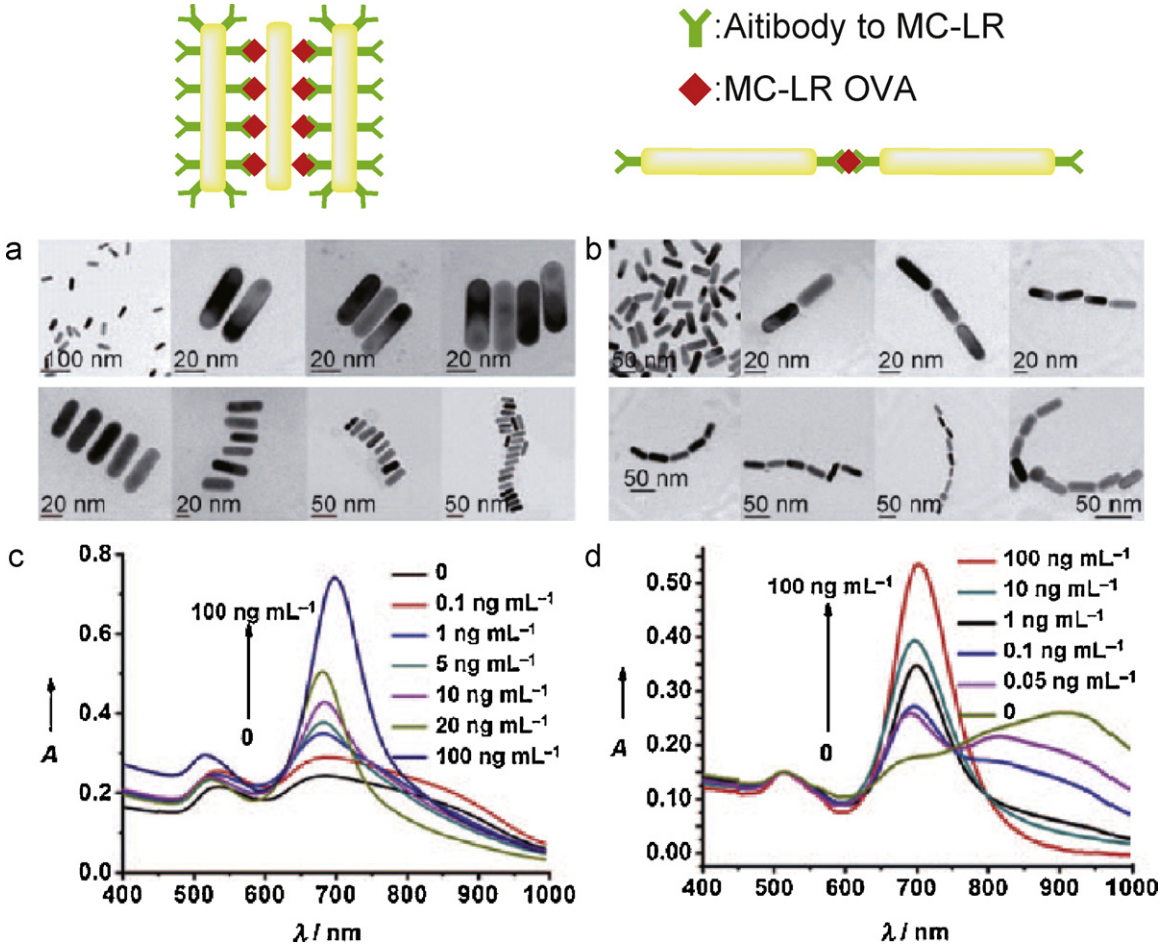

Fig. 10. TEM images of (a) side-to-side and (b) end-to-end nanorod assemblies with the respective SPR spectra (c and d) of Au nanorods upon an increase in the concentration of microcystin-LR (MC-LR).
Adapted from ref. [158] with permission from JWS.

tissues by the low-energy absorption of NIR light to normal tissues. However, the clinical use of AuNRs has been limited because of the liver accumulation of AuNRs and the cytotoxicity caused by CTAB used in a synthesis procedure and existing on the surface of AuNRs. This disadvantage has been masterfully overcome by changing the synthesis route and ligand exchange [144,165–167]. Choi and co-workers have developed an effective hyperthermia system in which AuNRs were capsulated into functional nanocarriers (chitosan-conjugated, pluronic-based nanocarriers). They have shown that the AuNR-loaded, chitosan-conjugated, and pluronic-based nanocarriers worked as imaging agents for cancer cells and as an effective hyperthermia agent for photothermal cancer therapy with NIR light exposure. The tumors developed in the mouse disappeared completely within 6 days after the photothermal therapy using chitosan-conjugated AuNRs, as shown in Fig. 11C.

5.3. Optical application using hollow nanostructures

The unique optical properties of noble-metal NPs can be attributed to the localized surface plasmon resonance (SPR), and the SPR peak position depends on the dielectric properties surrounding the NPs. A red-shift in the SPR peak is found as the refractive index of the surrounding medium increases, and the sensitive factor *S* is measured by the shift in the wavelength of the SPR peak per unit change in the refractive index (RIU) [47]. Solid gold nanospheres, nanocubes, and nanorods have *S* factors of approximately 40, 80, and 150–283 nm/RIU, respectively, while the *S* factor of a hollow cube with a wall length of 51 nm and wall thickness of 10 nm is found to be 620 nm/RIU [47]. The factor of gold nanorods is 150–263 nm/RIU, while a rod-shaped gold nanorattle is 285 nm/RIU [168]. The relatively large efficiency is attributed to the strong plasmonic fields resulting from the coupling between the external and the internal surface plasmon fields in the hollow nanostructures. A magnetic and plasmonic (wavelength: 700–800 nm) hollow gold nanostructure has been prepared by trapping iron oxide into a hollow space, while the surface has the anchorage sites of gold [169].

Surface Raman scattering (SERS) provides a powerful sensing platform, and gold and silver NPs are inserted into living cells to measure the distribution of biological molecules within the cells [170]. Here, silver NPs are most frequently used for activating the highly sensitive detection mode. However, aggregation of the NPs is necessary for a large signal enhancement, and the difficulty in controlling the aggregation shape and size of the NPs leads to the poor homogeneity of sensing. Hollow gold nanospheres reportedly lead to an approximately 10-fold improvement in signal consistency over standard silver NPs with respect to the peak intensity ratio [171]. Antibody-conjugated hollow gold nanospheres were used for the SER imagining of cancer makers, resulting in better homogeneous scattering properties than those of conjugated silver NPs [172].

5.4. Magnetic NP-assisted biosensors

Magnetic NPs (Fe_3O_4, FePt) functionalized by biomaterials have been extensively applied in a broad variety of bioelectronic applications [173,174]. The advantages of using magnetic NPs are high

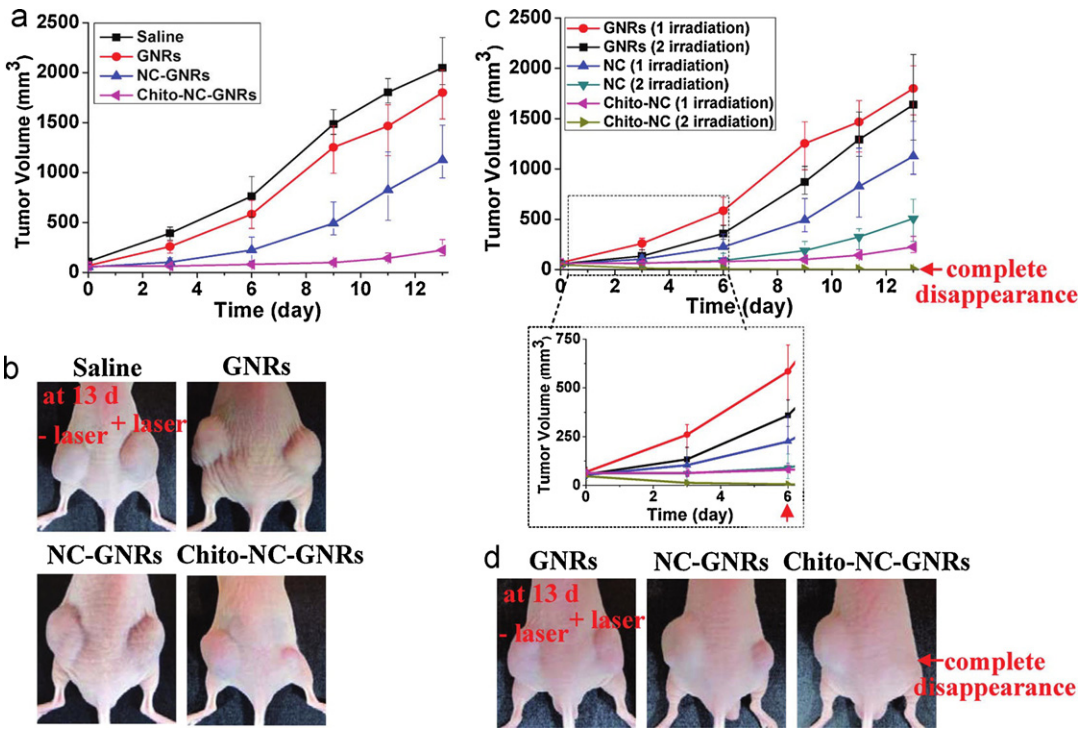

Fig. 11. (a) Changes in tumor volumes with respect to time and (b) the tumor images after irradiation of NIR laser for 4 min at 24 h after the intravenous injection of the nanomaterials. (c) Changes in tumor volumes and (d) the tumor images after NIR laser irradiations at 24 and 48 h after single intravenous injection of the nanomaterials. Reprinted with permission from ref. [143].

separation and resumption ability. In fact, multifunctional NPs that possess both magnetic properties and NIR absorption have a great potential for use in magnetic resonance imaging (MRI) [175], diagnosis, NIR photothermal ablation, pathogene detection [176], remote control of cellular behavior [177], and target delivery [178]. Wang et al. synthesized Fe_3O_4-fixed AuNRs in which Fe_3O_4 was assembled onto either the ends or both the ends and the sides of AuNRs. Interestingly, Fe_3O_4-attached AuNRs exhibit nanodumbell (fixed portion: ends of AuNRs) and necklace-like structures (fixed portion: ends and sides of AuNRs). They have successfully applied their assemblies to the dual-mode imaging and photothermal ablation of cancer cells [179] and pathogene detection [180].

5.5. Biosensors using AuNP array

We have recently succeeded in developing an electrical DNA sensor system based on the molecular conductivity of DNA using an array fabricated with a 50-nm AuNP and 1,10-decanedithiol, the latter was used for creating a nanometer-sized gap between the nanoparticles. The array was composed of repeated AuNP–alkyl chain–AuNP sequences on an insulator substrate (Fig. 12A). The assembling process used here has received considerable attention as one of the most promising techniques to construct such a nanometer-sized gap in nanoparticle networks [88,97,98,101]. The array was deposited on an interdigital microelectrode by submerging the electrode alternately in decanedithiol solution and aqueous AuNP dispersion. The interdigital electrode consists of two rows of 65 fingers of Pt electrodes spaced 5 μm apart and is fabricated on a quartz glass plate. These repeated deposition cycles produced an array film with an equally spaced nanometer-sized gap created by the binder molecule. The gap interval between each particle can be adjusted according to the length of the alkylchain of dithiol (ca. 1.3 nm); the resistance of the array (30 Ω cm) is comparable to the value of 20 Ω cm reported by Han et al. for nonanedithiol (ca. 1.1 nm) [181,182].

A single-strand DNA (*ss*DNA) probe (12-mer) with a sulfur head group at the 5′-phosphate end was fixed between the two nanoparticles to bind the sample DNA by hybridization. After the probe DNA modification onto AuNPs, target *ss*DNA dissolved in a TE buffer was added to the probe-modified AuNP array. Upon the sample addition, a resistance decrease was immediately observed with an *S*/*N* ratio of more than 40, followed by a steady-state resistance within 2 min (Fig. 12B). After the sample addition, hybridization occurred with the probe DNA, which was modified on the AuNP film, between adjacent AuNPs, as shown in Fig. 12C. The formation of a DNA double strand between NPs accelerates the electron transfer, which may induce a decrease in the film resistance. The magnitude of the response depended on the number of mismatched base pairs (bp) in the DNA strands, and the largest response among the samples was produced by the complementary strand. An increase in the number of mismatches led to a decrease in the response, and the 11-bp mismatched DNA exhibited the smallest response. The resistance changed in a nonlinear fashion with respect to the number of mismatches, implying that the presence of a 1-bp mismatch, an important diagnostic criterion for detecting single nucleotide polymorphisms (SNPs), was amplified [183–185]. Such differences in the resistance change may contribute to the conductivity of the double-strand DNA.

Hihath et al. have measured the conductivity of fully matched and mismatched strands located between a Au substrate and an STM tip [186]. The conductivity of the 1-bp mismatched strand was one order of magnitude lower than that of the fully matched strand. Furthermore, a 2-bp mismatch decreased the conductivity of a DNA sequence by two orders of magnitude. These results agree with our observation described above, confirming the role of DNA conductivity in resistance changes with respect to the number of mismatched bps. In order to verify that the hybridization causes the resistance

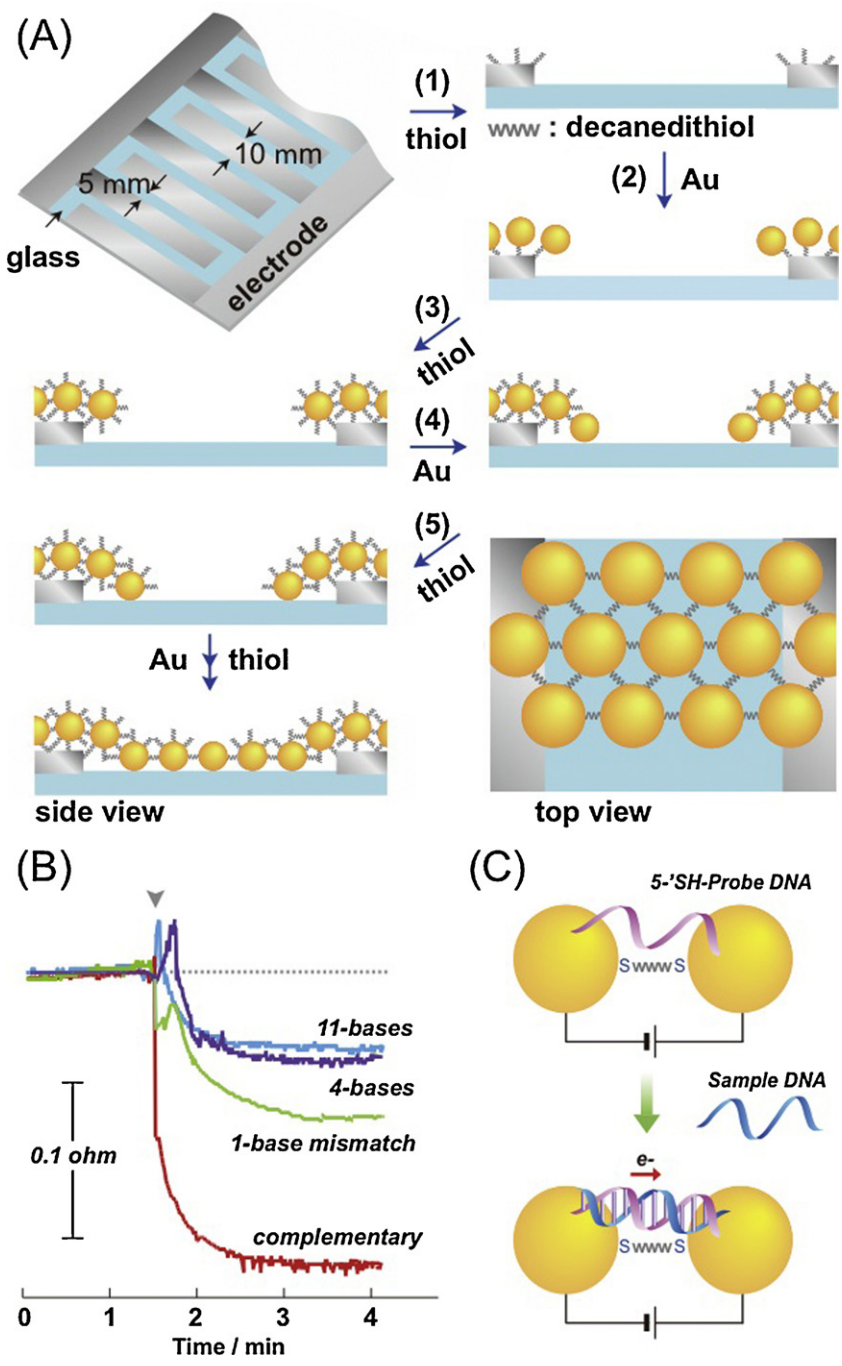

Fig. 12. (A) Procedures for fabrication of a gold nanoparticle array. Sequential immersion of an interdigital electrode into thiol and gold nanoparticle solutions leads to an AuNP array in which particles are inter-linked with an alkylchain of the binder. (B) Time course of resistance changes in the AuNP film caused by hybridization of probe, modified on the film, and target DNA, indicating the possibility of single nucleotide polymorphism detection. (C) Illustration of sensor electrodes before and after hybridization. Adapted from ref. [185] with permission from ACS.

changes, we also studied the effect of DNase I (from bovine pancreas), an enzyme that randomly breaks down DNA strands at their phosphodiester bonds [182].

In order to increase the sensor sensitivity, we have introduced a bridge substructure in the AuNP array consisting of 46- and 12-nm AuNPs (Fig. 13A). The substructure was formed between the 46-nm particles to anchor 12-nm AuNP probes (A and B), on which 12-nm oligomers were immobilized. The feasibility of this array structure as a new electrical sensing platform was examined. Upon the addition of a 24-mer target oligomer, the hybridization of the target with two 12-mer probes occurred close to the bridge, creating an additional circuit [187]. This sensor worked over a wide concentration range with a detection limit of 5.0 fmol, resulting in sensitivity that is 1000 times as high as that of a single particle system (Fig. 13B and C). Bridged hybridization occurred between the adjacent particles, and the resultant conductivity change may account for the direct electron transfer between the probe particles as well as the molecular conductivity of DNA [186,188–196]. These coupled effects would lead to a dramatic improvement in the detection limit by three orders of magnitude when the sensitivity

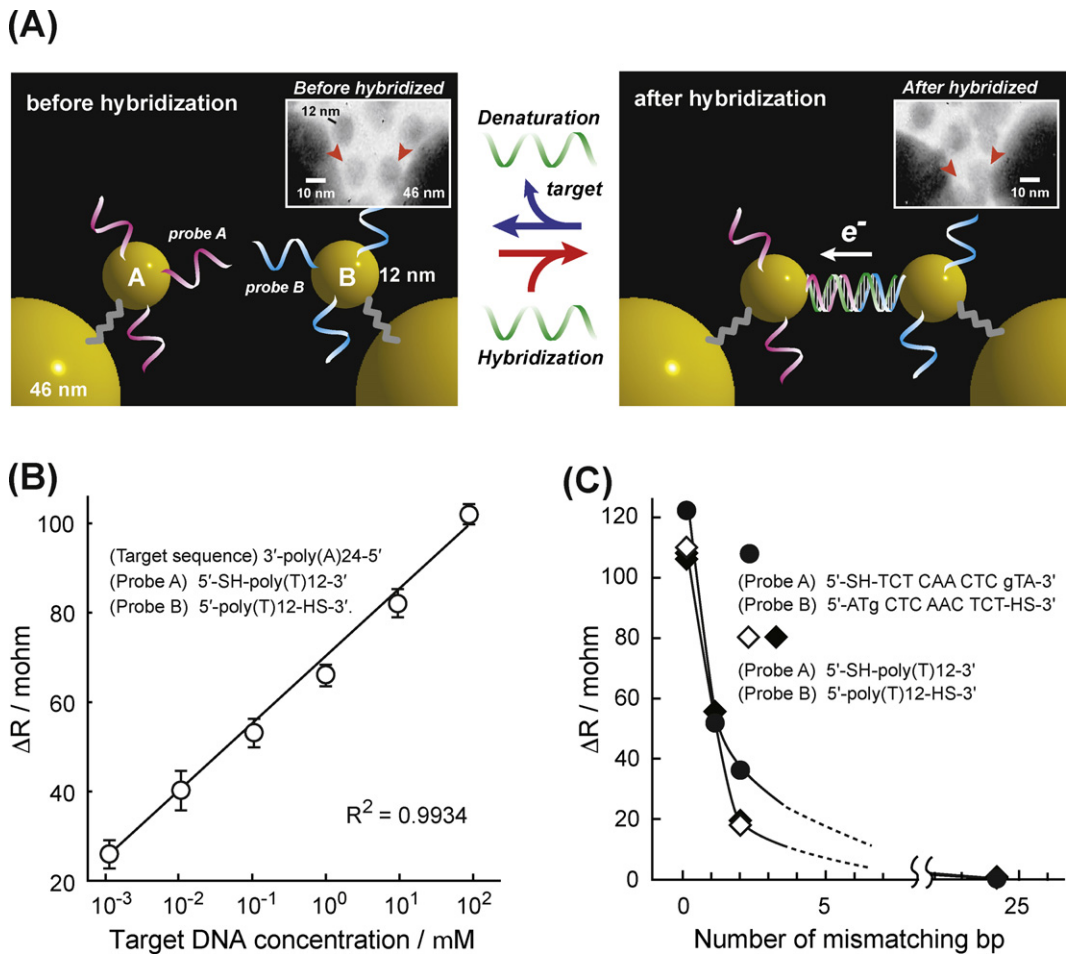

Fig. 13. (A) Conceptual illustrations of an open-bridge-structured gold nanoparticle array for label-free DNA detection. The array comprises 46-nm particles and the DNA-capped 12-nm AuNP probes, (A and B), immobilized on the 46-nm particles with dithiol. Probe DNA and complementary target DNA hybridization results in a complete bridge structure between 12-nm nanoparticles. The inset represents TEM images of the AuNP array, revealing 46-nm particles before and after hybridization. (B) Dependence of the sensor response on the target DNA concentration. (C) Sensor response versus the number of mismatched base pairs in the target DNA. The sensor array enables the detection of random sequences and SNPs.

Adapted from ref. [187] with permission from ACS.

is compared to that of a single-AuNP array system. On the basis of these findings, the technique discussed here shows potential for use in a wide variety of applications, not only for DNA analysis but also for the quantification of other molecules, using the conductivities of AuNPs as a new class of sensing platform.

6. Conclusions and future outlook

In this review, some recent bioanalytical applications based on the progressives of specific-shapes of metallic nanostructures have been described. Most of them can be backed up by their easy synthesis with several preparation methods in which the shape and morphology of the nanostructures can be controlled easily. Furthermore, the chemical adsorption between coinage NPs and thiol is one of the most important factors affecting the formation of NP assemblies and sensor devices for molecularly recognition, biological, and environmental applications. In fact, regularly arrayed AuNPs have been applied to various organic-vapor and biomolecule sensors since they provide the nanospace required for the analyte receptor with the thiol or amino group derivatized linker molecule. These developments may enable the realization of a high-density and high-throughput sensing platform for bio-associated materials such as DNA, antigens, and enzymatic reactions.

The scientific interest in metallic NPs, including that in the optical, magnetic, electronic, catalytic, and biomedical applications of these NPs, has not faded over time, and many physical and scientific papers are still published on this topic even though the usage and discovery of such NPs date back to thousands of years ago. The findings of these studies must hold a key to the development of the fields of nanoscience and nanotechnology in the future.

References

[1] Y. Xia, Y.J. Xiong, B. Lim, S.E. Skrabalak, Angew Chem. Int. Ed. 48 (2009) 60.
[2] M. Auffan, J. Rose, J.Y. Bottero, G.V. Lowry, J.P. Jolivet, M.R. Wiesner, Nat. Nanotechnol. 4 (2009) 634.
[3] C.L. Xu, L.B. Wang, W. Ma, L.G. Xu, W. Chen, Y.Y. Zhu, N.A. Kotov, Mat. Sci. Eng. R 70 (2010) 265.
[4] K.M. Mayer, J.H. Hafner, Chem. Rev. 111 (2011) 3828.
[5] J. Cheon, J.H. Lee, Acc. Chem. Res. 41 (2008) 1630.
[6] Y.W. Lin, C.C. Huang, H.T. Chang, Analyst 136 (2011) 863.
[7] J. Turkevitch, P.C. Stevenson, J. Hillier, Discuss. Faraday Soc. 11 (1951) 55.
[8] J. Polte, T.T. Ahner, F. Delissen, S. Sokolov, F. Emmerling, A.F. Thunemann, R. Kraehnert, J. Am. Chem. Soc. 132 (2010) 1296.
[9] M. Brust, M. Walker, D. Bethell, D.J. Schiffrin, R. Whyman, J. Chem. Soc. Chem. Commun. (1994) 801.
[10] M. Brust, J. Fink, D. Bethell, D.J. Schiffrin, C. Kiely, J. Chem. Soc. Chem. Commun. (1995) 1655.
[11] N.R. Jana, L. Gearheart, C.J. Murphy, Adv. Mater. 13 (2001) 1389.
[12] S.S. Chang, C.W. Shih, C.D. Chen, W.C. Lai, C.R.C. Wang, Langmuir 15 (1999) 701.
[13] Y.Y. Yu, S.S. Chang, C.L. Lee, C.R.C. Wang, J. Phys. Chem. B 101 (1997) 6661.

[14] F. Kim, J.H. Song, P.D. Yang, J. Am. Chem. Soc. 124 (2002) 14316.
[15] E. Leontidis, K. Kleitou, T. Kyprianidou-Leodidou, V. Bekiari, P. Lianos, Langmuir 18 (2002) 3659.
[16] O.R. Miranda, T.S. Ahmadi, J. Phys. Chem. B 109 (2005) 15724.
[17] T.S. Ahmadi, O.R. Miranda, N.R. Dollahon, Cryst. Growth Des. 6 (2006) 2747.
[18] B. Nikoobakht, M.A. El-Sayed, Chem. Mater. 15 (2003) 1957.
[19] C.J. Murphy, T.K. San, A.M. Gole, C.J. Orendorff, J.X. Gao, L. Gou, S.E. Hunyadi, T. Li, J. Phys. Chem. B 109 (2005) 13857.
[20] N.R. Jana, L. Gearheart, C.J. Murphy, J. Phys. Chem. B 105 (2001) 4065.
[21] M.A. El-Sayed, X.H. Huang, S. Neretina, Adv. Mater. 21 (2009) 4880.
[22] T. Niidome, M. Yamagata, Y. Okamoto, Y. Akiyama, H. Takahashi, T. Kawano, Y. Katayama, Y. Niidome, J. Control. Release 114 (2006) 343.
[23] Y. Niidome, K. Honda, K. Higashimoto, H. Kawazumi, S. Yamada, N. Nakashima, Y. Sasaki, Y. Ishida, J. Kikuchi, Chem. Commun. (2007) 3777.
[24] L. Tong, Q.S. Wei, A. Wei, J.X. Cheng, Photochem. Photobiol. 85 (2009) 21.
[25] J.J. Zhang, Y.G. Liu, L.P. Jiang, J.J. Zhu, Electrochem. Commun. 10 (2008) 355.
[26] C.C. Li, K.L. Shuford, Q.H. Park, W.P. Cai, Y. Li, E.J. Lee, S.O. Cho, Angew Chem. Int. Ed. 46 (2007) 3264.
[27] D. Seo, C. Il Yoo, I.S. Chung, S.M. Park, S. Ryu, H. Song, J. Phys. Chem. C 112 (2008) 2469.
[28] F. Kim, S. Connor, H. Song, T. Kuykendall, P.D. Yang, Angew Chem. Int. Ed. 43 (2004) 3673.
[29] C.J. Huang, P.H. Chiu, Y.H. Wang, W.R. Chen, T.H. Meen, J. Electrochem. Soc. 153 (2006) D129.
[30] D. Seo, J.C. Park, H. Song, J. Am. Chem. Soc. 128 (2006) 14863.
[31] Y. Kim do, T. Yu, E.C. Cho, Y. Ma, O.O. Park, Y. Xia, Angew Chem. Int. Ed. Engl. 50 (2011) 6328.
[32] Z.D. Wang, J.Q. Zhang, J.M. Ekman, P.J.A. Kenis, Y. Lu, Nano Lett. 10 (2010) 1886.
[33] S.E. Skrabalak, J. Chen, L. Au, X. Lu, X. Li, Y. Xia, Adv. Mater. 19 (2007) 3177.
[34] P.K. Jain, I.H. El-Sayed, M.A. El-Sayed, Nano Today 2 (2007) 18.
[35] A.I. Henry, J.M. Bingham, E. Ringe, L.D. Marks, G.C. Schatz, R.P. Van Duyne, J. Phys. Chem. C 115 (2011) 9291.
[36] Y.S. Huh, A.J. Lowe, A.D. Strickland, C.A. Batt, D. Erickson, J. Am. Chem. Soc. 131 (2009) 2208.
[37] A. Nagy, G. Mestl, Appl. Catal. a-Gen. 188 (1999) 337.
[38] Y.G. Sun, Y.N. Xia, Science 298 (2002) 2176.
[39] A.R. Siekkinen, J.M. McLellan, J. Chen, Y. Xia, Chem. Phys. Lett. 432 (2006) 491.
[40] S.E. Skrabalak, L. Au, X. Li, Y. Xia, Nat. Protoc. 2 (2007) 2182.
[41] S.E. Skrabalak, J. Chen, Y. Sun, X. Lu, L. Au, C.M. Cobley, Y. Xia, Acc. Chem. Res. 41 (2008) 1587.
[42] Y.G. Sun, B. Wiley, Z.Y. Li, Y.N. Xia, J. Am. Chem. Soc. 126 (2004) 9399.
[43] Y.A. Xia, L. Au, Y.C. Chen, F. Zhou, P.H.C. Camargo, B. Lim, Z.Y. Li, D.S. Ginger, Nano Res. 1 (2008) 441.
[44] G.S. Metraux, Y.C. Cao, R.C. Jin, C.A. Mirkin, Nano Lett. 3 (2003) 519.
[45] M. McEachran, D. Keogh, B. Pietrobon, N. Cathcart, I. Gourevich, N. Coombs, V. Kitaev, J. Am. Chem. Soc. 133 (2011) 8066.
[46] J. Chen, B. Wiley, Z.Y. Li, D. Campbell, F. Saeki, H. Cang, L. Au, J. Lee, X. Li, Y. Xia, Adv. Mater. 17 (2005) 2255.
[47] M.A. Mahmoud, M.A. El-Sayed, J. Am. Chem. Soc. 132 (2010) 12704.
[48] H. Zhang, M. Jin, H. Liu, J. Wang, M.J. Kim, D. Yang, Z. Xie, J. Liu, Y. Xia, ACS Nano 5 (2011) 8212.
[49] M.C. Daniel, D. Astruc, Chem. Rev. 104 (2004) 293.
[50] I. Srnova-Sloufova, B. Vlckova, Z. Bastl, T.L. Hasslett, Langmuir 20 (2004) 3407.
[51] H.Z. Shi, L.D. Zhang, W.P. Cai, J. Appl. Phys. 87 (2000) 1572.
[52] T. Shibata, B.A. Bunker, Z. Zhang, D. Meisel, C.F. Vardeman II, J.D. Gezelter, J. Am. Chem. Soc. 124 (2002) 11989.
[53] S. Tokonami, N. Morita, K. Takasaki, N. Toshima, J. Phys. Chem. C 114 (2010) 10336.
[54] Q.H.L. Xu, H.J. Jiang, T. Akita, T. Ishida, M. Haruta, J. Am. Chem. Soc. 133 (2011) 1304.
[55] N. Toshima, R. Ito, T. Matsushita, Y. Shiraishi, Catal. Today 122 (2007) 239.
[56] N. Toshima, T. Matsushita, Y. Shiraishi, S. Horiuchi, B Chem. Soc. Jpn. 80 (2007) 1217.
[57] M.J. Hostetler, C.J. Zhong, B.K.H. Yen, J. Anderegg, S.M. Gross, N.D. Evans, M. Porter, R.W. Murray, J. Am. Chem. Soc. 120 (1998) 9396.
[58] M.P. Mallin, C.J. Murphy, Nano Lett. 2 (2002) 1235.
[59] Y. Ma, W. Li, E.C. Cho, Z. Li, T. Yu, J. Zeng, Z. Xie, Y. Xia, ACS Nano 4 (2010) 6725.
[60] T. Ming, L. Zhao, Z. Yang, H. Chen, L. Sun, J. Wang, C. Yan, Nano Lett. 9 (2009) 3896.
[61] B.N. Wanjala, J. Luo, R. Loukrakpam, B. Fang, D. Mott, P.N. Njoki, M. Engelhard, H.R. Naslund, J.K. Wu, L.C. Wang, O. Malis, C.J. Zhong, Chem. Mater. 22 (2010) 4282.
[62] C.H. Wong, C.H. Liang, C.C. Wang, Y.C. Lin, C.H. Chen, C.Y. Wu, Anal. Chem. 81 (2009) 7750.
[63] M. Kumagai, T.K. Sarma, H. Cabral, S. Kaida, M. Sekino, N. Herlambang, K. Osada, M.R. Kano, N. Nishiyama, K. Kataoka, Macromol. Rapid Commun. 31 (2010) 1521.
[64] C.J. Zhong, L.Y. Wang, H.Y. Park, S.I.I. Lim, M.J. Schadt, D. Mott, J. Luo, X. Wang, J. Mater. Chem. 18 (2008) 2629.
[65] S. Neretina, E.C. Dreaden, W. Qian, M.A. El-Sayed, R.A. Hughes, J.S. Preston, P. Mascher, Nano Lett. 9 (2009) 3772.
[66] W. Ni, H. Chen, J. Su, Z. Sun, J. Wang, H. Wu, J. Am. Chem. Soc. 132 (2010) 4806.
[67] H.W. Huang, C.T. Qu, X.Y. Liu, S.W. Huang, Z.J. Xu, B. Liao, Y.L. Zeng, P.K. Chu, ACS Appl. Mater. Inter. 3 (2011) 183.
[68] F. Auzel, Chem. Rev. 104 (2004) 139.
[69] F. Wang, Y. Han, C.S. Lim, Y.H. Lu, J. Wang, J. Xu, H.Y. Chen, C. Zhang, M.H. Hong, X.G. Liu, Nature 463 (2010) 1061.
[70] J. Zhou, Y. Sun, X.X. Du, L.Q. Xiong, H. Hu, F.Y. Li, Biomaterials 31 (2010) 3287.
[71] H. Zhang, Y.J. Li, I.A. Ivanov, Y.Q. Qu, Y. Huang, X.F. Duan, Angew Chem. Int. Ed. 49 (2010) 2865.
[72] J.A. Tang, D.P. Tang, B.L. Su, J.X. Huang, B. Qiu, G.N. Chen, Biosens. Bioelectron. 26 (2011) 3219.
[73] G. Lai, F. Yan, H. Ju, Anal. Chem. 81 (2009) 9730.
[74] Y. Liang, Y. Li, H. Wang, J. Zhou, J. Wang, T. Regier, H. Dai, Nat. Mater. 10 (2011) 780.
[75] H. Wang, Y. Yang, Y. Liang, J.T. Robinson, Y. Li, A. Jackson, Y. Cui, H. Dai, Nano Lett. 11 (2011) 2644.
[76] Y. Xia, W. Li, C.M. Cobley, J. Chen, X. Xia, Q. Zhang, M. Yang, E.C. Cho, P.K. Brown, Acc. Chem. Res. 44 (2011) 914.
[77] Y. Du, S. Guo, H. Qin, S. Dong, E. Wang, Chem. Commun. (Camb) (2011).
[78] R.D. Tyagi, X.L. Zhang, S. Yan, R.Y. Surampalli, Chemosphere 82 (2011) 489.
[79] B. Nair, T. Pradeep, Cryst. Growth Des. 2 (2002) 293.
[80] V.S. Coker, J.A. Bennett, N.D. Telling, T. Henkel, J.M. Charnock, G. van der Laan, R.A.D. Pattrick, C.I. Pearce, R.S. Cutting, I.J. Shannon, J. Wood, E. Arenholz, I.C. Lyon, J.R. Lloyd, ACS Nano 4 (2010) 2577.
[81] U. Leonhardt, Nat. Photonics 1 (2007) 207.
[82] G. Mie, Ann. Physik 25 (1908) 377.
[83] S. Link, Z.L. Wang, M.A. El-Sayed, J. Phys. Chem. B 103 (1999) 3529.
[84] B. Rodriguez-Gonzalez, A. Sanchez-Iglesias, M. Giersig, L.M. Liz-Marzan, Faraday Discuss. 125 (2004) 133.
[85] E. Hao, G.C. Schatz, J.T. Hupp, J. Fluoresc. 14 (2004) 331.
[86] M. Rycenga, C.M. Cobley, J. Zeng, W. Li, C.H. Moran, Q. Zhang, D. Qin, Y. Xia, Chem. Rev. 111 (2011) 3669.
[87] A. Stein, F. Li, D.P. Josephson, Angew Chem. Int. Ed. 50 (2011) 360.
[88] H. Shiigi, Y. Yamamoto, N. Yoshi, H. Nakao, T. Nagaoka, Chem. Commun. (2006) 4288.
[89] H. Shiigi, R. Morita, Y. Yamamoto, S. Tokonami, H. Nakao, T. Nagaoka, Chem. Commun. (Camb) (2009) 3615.
[90] C.Y. Song, G.P. Zhao, P.J. Zhang, N.L. Rosi, J. Am. Chem. Soc. 132 (2010) 14033.
[91] D. Zerrouki, J. Baudry, D. Pine, P. Chaikin, J. Bibette, Nature 455 (2008) 380.
[92] M.E. Leunissen, R. Dreyfus, F.C. Cheong, D.G. Grier, R. Sha, N.C. Seeman, P.M. Chaikin, Nat. Mater. 8 (2009) 590.
[93] K.K. Caswell, J.N. Wilson, U.H. Bunz, C.J. Murphy, J. Am. Chem. Soc. 125 (2003) 13914.
[94] G.A. Devries, M. Brunnbauer, Y. Hu, A.M. Jackson, B. Long, B.T. Neltner, O. Uzun, B.H. Wunsch, F. Stellacci, Science 315 (2007) 358.
[95] Z. Nie, D. Fava, E. Kumacheva, S. Zou, G.C. Walker, M. Rubinstein, Nat. Mater. 6 (2007) 609.
[96] K. Liu, Z. Nie, N. Zhao, W. Li, M. Rubinstein, E. Kumacheva, Science 329 (2010) 197.
[97] H. Shiigi, Y. Yamamoto, H. Yakabe, S. Tokonami, T. Nagaoka, Chem. Commun. (2003) 1038.
[98] Y. Yamamoto, H. Shiigi, T. Nagaoka, Electroanalysis 17 (2005) 2224.
[99] H. Shiigi, Y. Yamamoto, S. Takeda, T. Nagaoka, J. Electrochem. Soc. 154 (2007) D462.
[100] H. Shiigi, N. Yoshi, Y. Yamamoto, M. Iwamoto, T. Nagaoka, Microelectron. Eng. 85 (2008) 1214.
[101] Y. Yamamoto, N. Yoshi, H. Shiigi, T. Nagaoka, Solid State Ionics 177 (2006) 2325.
[102] I. Hussain, Z. Wang, A.I. Cooper, M. Brust, Langmuir 22 (2006) 2938.
[103] C.M. McIntosh, E.A. Esposito, A.K. Boal, J.M. Simard, C.T. Martin, V.M. Rotello, J. Am. Chem. Soc. 123 (2001) 7626.
[104] T. Yonezawa, S.Y. Onoue, N. Kimizuka, Chem. Lett. 31 (2002) 1172.
[105] V.J. Gandubert, R.B. Lennox, Langmuir 21 (2005) 6532.
[106] H. Nakao, M. Gad, S. Sugiyama, K. Otobe, T. Ohtani, J. Am. Chem. Soc. 125 (2003) 7162.
[107] H. Nakao, H. Shiigi, Y. Yamamoto, S. Tokonami, T. Nagaoka, S. Sugiyama, T. Ohtani, Nano Lett. 3 (2003) 1391.
[108] H. Nakao, Anal. Sci. 25 (2009) 1387.
[109] M.G. Warner, J.E. Hutchison, Nat. Mater. 2 (2003) 272.
[110] Y.Y. Pinto, J.D. Le, N.C. Seeman, K. Musier-Forsyth, T.A. Taton, R.A. Kiehl, Nano Lett. 5 (2005) 2399.
[111] M.R. Jones, R.J. Macfarlane, B. Lee, J. Zhang, K.L. Young, A.J. Senesi, C.A. Mirkin, Nat. Mater. 9 (2010) 913.
[112] A. Faccenda, C.A. Bonham, P.O. Vacratsis, X. Zhang, B. Mutus, J. Am. Chem. Soc. 132 (2010) 11392.
[113] M.S. Yavuz, Y. Cheng, J. Chen, C.M. Cobley, Q. Zhang, M. Rycenga, J. Xie, C. Kim, K.H. Song, A.G. Schwartz, L.V. Wang, Y. Xia, Nat. Mater. 8 (2009) 935.
[114] W. Li, X. Cai, C. Kim, G. Sun, Y. Zhang, R. Deng, M. Yang, J. Chen, S. Achilefu, L.V. Wang, Y. Xia, Nanoscale 3 (2011) 1724.
[115] C. Radhakumary, K. Sreenivasan, Anal. Chem. 83 (2011) 2829.
[116] T. Endo, K. Kerman, N. Nagatani, H.M. Hiepa, D.K. Kim, Y. Yonezawa, K. Nakano, E. Tamiya, Anal. Chem. 78 (2006) 6465.
[117] W. Shenton, S.A. Davis, S. Mann, Adv. Mater. 11 (1999) 449.
[118] J.F. Hainfeld, R.D. Powell, G.W. Hacker, C.M. Niemeyer, C.A. Mirkin, Nanobiotechnology, VCH, Weinheim, 2004, p. 353.
[119] N. Uehara, Anal. Sci. 26 (2010) 1219.
[120] C.A. Mirkin, R.L. Letsinger, R.C. Mucic, J.J. Storhoff, Nature 382 (1996) 607.
[121] Z. Li, R.C. Jin, C.A. Mirkin, R.L. Letsinger, Nucleic Acids Res. 30 (2002) 1558.
[122] S.J. Hurst, H.D. Hill, C.A. Mirkin, J. Am. Chem. Soc. 130 (2008) 12192.
[123] J.S. Kim, Y.R. Kim, R.K. Mahajan, H. Kim, ACS Appl. Mater. Inter. 2 (2010) 292.

[124] C.J. Mu, D.A. LaVan, R.S. Langer, B.R. Zetter, ACS Nano 4 (2010) 1511.
[125] F.Y. Yu, B.H. Liu, Z.J. Tsao, J.J. Wang, Anal. Chem. 80 (2008) 7029.
[126] P.C. Ray, G.K. Darbha, A.K. Singh, U.S. Rai, E. Yu, H.T. Yu, J. Am. Chem. Soc. 130 (2008) 8038.
[127] P.C. Ray, S.S.R. Dasary, A.K. Singh, D. Senapati, H.T. Yu, J. Am. Chem. Soc. 131 (2009) 13806.
[128] X.Y. Xu, W.L. Daniel, W. Wei, C.A. Mirkin, Small 6 (2010) 623.
[129] H. Xu, X. Mao, Q.X. Zeng, S.F. Wang, A.N. Kawde, G.D. Liu, Anal. Chem. 81 (2009) 669.
[130] X. Mao, Y.Q. Ma, A.G. Zhang, L.R. Zhang, G.D. Liu, L.W. Zeng, Anal. Chem. 81 (2009) 1660.
[131] D. Mazumdar, J.W. Liu, G. Lu, J.Z. Zhou, Y. Lu, Chem. Commun. 46 (2010) 1416.
[132] X.H. Wang, T. Liu, N. Xu, Y. Zhang, S. Wang, Anal. Bioanal. Chem. 389 (2007) 903.
[133] M.H.V. Werts, N. Nerambourg, M. Charlot, M. Blanchard-Desce, Langmuir 23 (2007) 5563.
[134] C. Sonnichsen, B.M. Reinhard, J. Liphardt, A.P. Alivisatos, Nat. Biotechnol. 23 (2005) 741.
[135] Y.W. Jun, S. Sheikholeslami, D.R. Hostetter, C. Tajon, C.S. Craik, A.P. Alivisatos, Proc. Natl. Acad. Sci. U.S.A. 106 (2009) 17735.
[136] B.M. Reinhard, S. Sheikholeslami, A. Mastroianni, A.P. Alivisatos, J. Liphardt, Proc. Natl. Acad. Sci. U.S.A. 104 (2007) 2667.
[137] M. Rex, F.E. Hernandez, A.D. Campiglia, Anal. Chem. 78 (2006) 445.
[138] H. Misawa, K. Ueno, S. Juodkazis, M. Mino, V. Mizeikis, J. Phys. Chem. C 111 (2007) 4180.
[139] J. Perez-Juste, B. Rodriguez-Gonzalez, P. Mulvaney, L.M. Liz-Marzan, Adv. Funct. Mater. 15 (2005) 1065.
[140] M. Das, N. Sanson, D. Fava, E. Kumacheva, Langmuir 23 (2007) 196.
[141] Y. Horiguchi, K. Honda, Y. Kato, N. Nakashima, Y. Niidome, Langmuir 24 (2008) 12026.
[142] Y. Choi, B. Jang, J.Y. Park, C.H. Tung, I.H. Kim, ACS Nano 5 (2011) 1086.
[143] W.I. Choi, J.Y. Kim, C. Kang, C.C. Byeon, Y.H. Kim, G. Tae, ACS Nano 5 (2011) 1995.
[144] W.C.W. Chan, T.S. Hauck, A.A. Ghazani, Small 4 (2008) 153.
[145] X.H. Huang, I.H. El-Sayed, W. Qian, M.A. El-Sayed, J. Am. Chem. Soc. 128 (2006) 2115.
[146] S. Sambhara, K.V. Chakravarthy, A.C. Bonoiu, W.G. Davis, P. Ranjan, H. Ding, R. Hu, J.B. Bowzard, E.J. Bergey, J.M. Katz, P.R. Knight, P.N. Prasad, Proc. Natl. Acad. Sci. U.S.A. 107 (2010) 10172.
[147] N. Khlebtsov, L. Dykman, Chem. Soc. Rev. 40 (2011) 1647.
[148] H.X. Xu, T. Shegai, Z.P. Li, T. Dadosh, Z.Y. Zhang, G. Haran, Proc. Natl. Acad. Sci. U.S.A. 105 (2008) 16448.
[149] Y.N. Xia, W.Y. Li, P.H.C. Camargo, X.M. Lu, Nano Lett. 9 (2009) 485.
[150] S.W. Kim, S. Kim, J.H. Jin, Y.J. Kim, I.Y. Park, Y. Kim, Nature 453 (2008) 757.
[151] W.E. Moerner, A. Kinkhabwala, Z.F. Yu, S.H. Fan, Y. Avlasevich, K. Mullen, Nat. Photonics 3 (2009) 654.
[152] H. Misawa, K. Ueno, S. Juodkazis, V. Mizeikis, K. Sasaki, Adv. Mater. 20 (2008) 26.
[153] A. Sundaramurthy, P.J. Schuck, N.R. Conley, D.P. Fromm, G.S. Kino, W.E. Moerner, Nano Lett. 6 (2006) 355.
[154] H. Misawa, K. Ueno, S. Juodkazis, T. Shibuya, Y. Yokota, V. Mizeikis, K. Sasaki, J. Am. Chem. Soc. 130 (2008) 6928.
[155] A.N. Grigorenko, N.W. Roberts, M.R. Dickinson, Y. Zhang, Nat. Photonics 2 (2008) 365.
[156] J.F. Wang, L. Shao, K.C. Woo, H.J. Chen, Z. Jin, H.Q. Lin, ACS Nano 4 (2010) 3053.
[157] K.G. Thomas, P. Pramod, Adv. Mater. 20 (2008) 4300.
[158] C.L. Xu, L.B. Wang, Y.Y. Zhu, L.G. Xu, W. Chen, H. Kuang, L.Q. Liu, A. Agarwal, N.A. Kotov, Angew Chem. Int. Ed. 49 (2010) 5472.
[159] E. Dulkeith, M. Ringler, T.A. Klar, J. Feldmann, A. Munoz Javier, W.J. Parak, Nano Lett. 5 (2005) 585.
[160] P.K. Jain, K.S. Lee, I.H. El-Sayed, M.A. El-Sayed, J. Phys. Chem. B 110 (2006) 7238.
[161] D.K. Yi, I.C. Sun, J.H. Ryu, H. Koo, C.W. Park, I.C. Youn, K. Choi, I.C. Kwon, K. Kim, C.H. Ahn, Bioconjug. Chem. 21 (2010) 2173.
[162] W.S. Kuo, C.N. Chang, Y.T. Chang, M.H. Yang, Y.H. Chien, S.J. Chen, C.S. Yeh, Angew Chem. Int. Ed. 49 (2010) 2711.
[163] G. von Maltzahn, A. Centrone, J.H. Park, R. Ramanathan, M.J. Sailor, T.A. Hatton, S.N. Bhatia, Adv. Mater. 21 (2009) 3175.
[164] C.L. Chen, L.R. Kuo, C.L. Chang, Y.K. Hwu, C.K. Huang, S.Y. Lee, K. Chen, S.J. Lin, J.D. Huang, Y.Y. Chen, Biomaterials 31 (2010) 4104.
[165] H. Takahashi, Y. Niidome, T. Niidome, K. Kaneko, H. Kawasaki, S. Yamada, Langmuir 22 (2006) 2.
[166] Y.M. Huh, E. Kim, J. Yang, J. Choi, J.S. Suh, S. Haam, Nanotechnology 20 (2009) 365602.
[167] S.N. Bhatia, G. von Maltzahn, J.H. Park, A. Agrawal, N.K. Bandaru, S.K. Das, M.J. Sailor, Cancer Res. 69 (2009) 3892.
[168] Y. Khalavka, J. Becker, C. Sönnichsen, J. Am. Chem. Soc. 131 (2009) 1871.
[169] C. Huang, J. Jiang, C. Muangphat, X. Sun, Y. Hao, Nanoscale Res. Lett. 6 (2011) 1.
[170] K. Kneipp, A.S. Haka, H. Kneipp, K. Badizadegan, N. Yoshizawa, C. Boone, K.E. Shafer-Peltier, J.T. Motz, R.R. Dasari, M.S. Feld, Appl. Spectrosc. 56 (2002) 150.
[171] A.M. Schwartzberg, T.Y. Oshiro, J.Z. Zhang, T. Huser, C.E. Talley, Anal. Chem. 78 (2006) 4732.
[172] S. Lee, H. Chon, M. Lee, J. Choo, S.Y. Shin, Y.H. Lee, I.J. Rhyu, S.W. Son, C.H. Oh, Biosens. Bioelectron. 24 (2009) 2260.
[173] I. Willner, E. Katz, Angew Chem. Int. Ed. Engl. 42 (2003) 4576.
[174] J. Xie, G. Liu, H.S. Eden, H. Ai, X. Chen, Acc. Chem. Res. 44 (2011) 883.
[175] J.H. Lee, Y.M. Huh, Y.W. Jun, J.W. Seo, J.T. Jang, H.T. Song, S. Kim, E.J. Cho, H.G. Yoon, J.S. Suh, J. Cheon, Nat. Med. 13 (2007) 95.
[176] X. Huang, K. El-Boubbou, C. Gruden, J. Am. Chem. Soc. 129 (2007) 13392.
[177] J. Dobson, Nat. Nanotechnol. 3 (2008) 139.
[178] Z. Medarova, W. Pham, C. Farrar, V. Petkova, A. Moore, Nat. Med. 13 (2007) 372.
[179] C.G. Wang, J. Chen, T. Talavage, J. Irudayaraj, Angew Chem. Int. Ed. 48 (2009) 2759.
[180] C.G. Wang, J. Irudayaraj, Small 6 (2010) 283.
[181] L. Han, D.R. Daniel, M.M. Maye, C.J. Zhong, Anal. Chem. 73 (2001) 4441.
[182] S. Tokonami, M. Iwamoto, K. Hashiba, H. Shiigi, T. Nagaoka, Solid State Ionics 177 (2006) 2317.
[183] S. Tokonami, H. Shiigi, T. Nagaoka, J. Electrochem. Soc. 155 (2008) J105.
[184] S. Tokonami, H. Shiigi, T. Nagaoka, Electroanalysis 20 (2008) 355.
[185] H. Shiigi, S. Tokonami, H. Yakabe, T. Nagaoka, J. Am. Chem. Soc. 127 (2005) 3280.
[186] J. Hihath, B.Q. Xu, P.M. Zhang, N.J. Tao, Proc. Natl. Acad. Sci. U.S.A. 102 (2005) 16979.
[187] S. Tokonami, H. Shiigi, T. Nagaoka, Anal. Chem. 80 (2008) 8071.
[188] D. Porath, A. Bezryadin, S. de Vries, C. Dekker, Nature 403 (2000) 635.
[189] H.W. Fink, C. Schonenberger, Nature 398 (1999) 407.
[190] A.Y. Kasumov, M. Kociak, S. Gueron, B. Reulet, V.T. Volkov, D.V. Klinov, H. Bouchiat, Science 291 (2001) 280.
[191] Y. Zhang, R.H. Austin, J. Kraeft, E.C. Cox, N.P. Ong, Phys. Rev. Lett. 89 (2002) 198102.
[192] C. Dekker, M.A. Ratner, Phys. World 14 (2001) 29.
[193] K.W. Hipps, Science 294 (2001) 536.
[194] H. Cohen, C. Nogues, R. Naaman, D. Porath, Proc. Natl. Acad. Sci. U.S.A. 102 (2005) 11589.
[195] E. Wierzbinski, J. Arndt, W. Hammond, K. Slowinski, Langmuir 22 (2006) 2426.
[196] B.Q. Xu, P.M. Zhang, X.L. Li, N.J. Tao, Nano Lett. 4 (2004) 1105.